Coupled snow cover and avalanche dynamics simulations to evaluate wet snow avalanche activity

Wever, Nander ; Vera Valero, César ; Techel, Frank

Abstract: We present physics-based snowpack simulations for four snow seasons with detailed wet snow avalanche activity records. The distributed, spatially explicit simulations using the Alpine3D and SNOWPACK model show that the simulated snowpack in the release areas of documented wet snow avalanches often exhibits its first wetting of the season on the release day. This first wetting is accompanied in the simulations by liquid water accumulating on capillary barriers, often formed by depth hoar layers. The strongest water accumulations and largest increases in percolation depth are found on the day of avalanche release. For individual avalanche paths, however, this only holds in 25-30% of the cases. Assuming that the depth of the strongest water accumulation corresponds to the avalanche fracture depth, the avalanche dynamics model RAMMS-Extended was run using simulated snowpack properties as initial conditions in the release area and boundary conditions along the avalanche path. On average, the simulated affected area by the avalanche and runout distance for the release day are statistically significant in closer agreement with the observations than two days before the release. This does not hold for the simulations of one day before and one and two days after the release. This suggests that fracture depths and the temporal evolution of percolation depths are adequately simulated within a ± 1 day period. The results show a large potential for distributed snow cover and avalanche dynamics simulations to assess wet snow avalanche hazards, although predictions for individual avalanche paths remain challenging.

DOI: https://doi.org/10.1029/2017JF004515

Journal of Geophysical Research: Earth Surface

RESEARCH ARTICLE
10.1029/2017JF004515

Coupled Snow Cover and Avalanche Dynamics Simulations to Evaluate Wet Snow Avalanche Activity

Nander Wever[1,2,3], **Cesar Vera Valero**[2,4], **and Frank Techel**[2,5]

[1]School of Architecture, Civil and Environmental Engineering, École Polytechnique Fédérale de Lausanne, Lausanne, Switzerland, [2]WSL Institute for Snow and Avalanche Research SLF, Davos, Switzerland, [3]Department of Atmospheric and Oceanic Sciences, University of Colorado Boulder, Boulder, CO, USA, [4]Wyssen Avalanche Control, Reichenbach, Switzerland, [5]Department of Geography, University of Zurich, Zurich, Switzerland

Abstract We present physics-based snowpack simulations for four snow seasons with detailed wet snow avalanche activity records. The distributed, spatially explicit simulations using the Alpine3D and SNOWPACK model show that the simulated snowpack in the release areas of documented wet snow avalanches often exhibits its first wetting of the season on the release day. This first wetting is accompanied in the simulations by liquid water accumulating on capillary barriers, often formed by depth hoar layers. The strongest water accumulations and largest increases in percolation depth are found on the day of avalanche release. For individual avalanche paths, however, this only holds in 25%–30% of the cases. Assuming that the depth of the strongest water accumulation corresponds to the avalanche fracture depth, the avalanche dynamics model RAMMS-Extended was run using simulated snowpack properties as initial conditions in the release area and boundary conditions along the avalanche path. On average, the simulated affected area by the avalanche and runout distance for the release day are statistically significant in closer agreement with the observations than two days before the release. This does not hold for the simulations of 1 day before and 1 and 2 days after the release. This suggests that fracture depths and the temporal evolution of percolation depths are adequately simulated within a ±1-day period. The results show a large potential for distributed snow cover and avalanche dynamics simulations to assess wet snow avalanche hazards, although predictions for individual avalanche paths remain challenging.

Plain Language Summary Recent years have shown an increasing interest in methods to forecast wet snow avalanches. Wet snow avalanche activity is closely related to water flow processes in snow. It is often considered that water accumulating on layer transitions inside the snowpack (e.g., layers with fine grains on top of coarse grains), may locally reduce snow strength and trigger an avalanche. We show results from detailed simulations of liquid water flow in snow in a mountainous area surrounding Davos, Switzerland, for which also detailed avalanche records are available. We find that periods with strong local water accumulations inside the snowpack correspond well with periods of avalanche activity. On average, the strongest water accumulations and the strongest increases in percolations depth in the simulations occur within 1 day of the observed avalanche activity. Assuming that the depth of the water accumulation is the fracture depth, avalanche simulations were carried out to assess the resulting avalanche size. Also, here a good correspondence was found between the average simulated and observed runout distances, suggesting that fracture depths are on average adequately simulated. However, for individual avalanche paths, errors in runout distance were regularly considerable, indicating that predictions for individual avalanche paths remain challenging.

Key Points:
- Detailed, distributed snow cover simulations were performed for a mountainous area for which detailed avalanche observations exist
- Snow cover simulations of water percolation and water ponding on capillary barriers correspond with observed wet snow avalanche activity
- Avalanche dynamics simulations driven by the simulated snow cover were partly able to predict the inundated area and runout distance

Supporting Information:
- Supporting Information S1

Correspondence to:
N. Wever,
nander.wever@colorado.edu

Citation:
Wever, N., Vera Valero, C., & Techel, F. (2018). Coupled snow cover and avalanche dynamics simulations to evaluate wet snow avalanche activity. *Journal of Geophysical Research: Earth Surface*, *123*, 1772–1796. https://doi.org/10.1029/2017JF004515

Received 9 OCT 2017
Accepted 13 JUN 2018
Accepted article online 22 JUN 2018
Published online 14 AUG 2018

1. Introduction

Wet snow avalanches are a recurring threat for settlements, transportation lines, and industrial and mining activities located in mountainous, snowy regions (Vera Valero et al., 2016; Zischg et al., 2005). An avalanche hazard assessment requires an estimation of the release probability as well as the size of the avalanche, often expressed via the runout distance (e.g., Canadian avalanche classification, McClung & Schaerer, 2006).

To predict wet snow avalanche activity, the water flow in snow needs to be assessed. However, release zones for wet snow avalanches are inherently dangerous to access for manual observations. Furthermore, the often

rapid changes in wet snow and the large spatial variability cause manual observations to rarely capture the right place and time (Techel & Pielmeier, 2011). Recent developments in using radar to monitor snow cover wetness (e.g., Heilig et al., 2015; Mitterer, Heilig, et al., 2011; Schmid et al., 2014) are promising, but not ready for wide-scale deployment. As a solution for the difficulties with in situ observations, numerical snow cover simulations using physics-based models have become increasingly important for predicting wet snow avalanche activity (Mitterer, Hirashima, & Schweizer, 2011; Mitterer & Schweizer, 2013; Wever, Vera Valero, & Fierz, 2016).

It is often considered that water accumulating on microstructural transitions inside the snowpack can locally reduce the shear strength of the snow considerably, leading to an avalanche release (Fierz & Föhn, 1994; Kattelmann, 1984; Mitterer, Hirashima, & Schweizer, 2011; Takeuchi & Hirashima, 2013). Wever, Vera Valero, & Fierz, (2016) showed that the simulation of such water accumulations inside the snowpack can identify periods with wet snow avalanche activity. Following the notion that the fracture initiating the avalanche release can occur in such layers, the study found that the depth of these accumulations correlated significantly with avalanche size. However, Techel and Pielmeier (2009) found in field observations that particularly the initial wetting of weak layers — soft, coarse-grained layers consisting of facetted and depth hoar grains — is associated with wet snow instability, even at low snow wetness. Although these results seem contradictory, typical weak layers often form marked microstructural transitions in the snowpack (i.e., a transition from fine- to coarse-grained snow) above which water may accumulate. Local water accumulations inside the snowpack may thereby indicate the presence of weak layers and that those layers have been reached by water. Durand et al. (1999) used the concept of the first wetting of weak layers in snowpack simulations as an indicator for forecasting wet snow avalanche activity.

Snowpack models may ultimately be able to provide an assessment of the snowpack state and successfully predict snowpack stability and release probabilities. However, these models do not consider the terrain potential and the affected areas after an avalanche release, which is determined by the local terrain topology and, for example, the presence of gullies or forested areas (Feistl et al., 2015; Fischer et al., 2012). Terrain analysis may provide potential release areas (Bühler et al., 2013; Maggioni & Gruber, 2003; Veitinger et al., 2016), but avalanche dynamics models, such as RAMMS-Extended (Vera Valero et al., 2018) or r.avaflow (Mergili et al., 2017) will be needed to assess the consequences, for example, runout distance, inundated area, and damaging potential, following an avalanche release.

At the same time, avalanche flow behavior depends on the initial and slab conditions as well as the snow cover properties along the avalanche path (Naaim et al., 2013; Steinkogler et al., 2014). Therefore, avalanche dynamics models also require snow cover information from the release zone and along the avalanche path. For example, the inclusion of lubrication by the presence of liquid water in the sliding surface, as well as the temperature effect on friction coefficients, was found to improve the simulation of runout distances and inundated areas by the model RAMMS-Extended (Vera Valero et al., 2015, 2016). However, as a result, the RAMMS-Extended model additionally requires initial conditions in the release area as well as boundary conditions along the avalanche path, given by the snowpack properties (snow temperature, liquid water content, and snow density).

The obvious solution is to use snowpack models to derive snowpack layering and stability in the release zones (Takeuchi & Hirashima, 2013; Vera Valero et al., 2016) to provide the initial and boundary conditions for avalanche dynamics models (Vera Valero et al., 2018). It may also be foreseen that future dynamic hazard mapping relies on a combination of snowpack models and avalanche dynamics models to nowcast or forecast avalanche hazards. A direct coupling between snow cover and avalanche dynamics models for dynamical hazard mapping based on current snowpack conditions is nowadays technically feasible, but the quality of the outcome heavily relies on the ability of the snowpack model to predict the snowpack stability and hence avalanche release probability. Generally, snowpack models were found to be able to predict wet snow avalanche days, albeit accompanied by a large false alarm rate (Bellaire et al., 2017; Mitterer & Schweizer, 2014). Second, an important initial condition for the avalanche dynamics model is the release area. Although potential release areas can be successfully depicted by terrain analysis, acquiring the actual release area as a function of snowpack properties remains challenging. In absence of a solution for both problems, we formulate here two aims for this study: (i) characterize the state of the snowpack in locations and at times when a wet snow avalanche released and compare these with conditions on days prior and after the day of avalanche release, and (ii) assess to what extent these simulated snowpack characteristics (particularly fracture depth) used as initial conditions for wet snow avalanche dynamics simulations can reproduce observed avalanche size.

To this end, we performed distributed simulations of the snowpack conditions in an area of about 460 km^2 surrounding Davos, Switzerland, using the physics-based snow cover model SNOWPACK within the distributed Alpine3D model (Lehning et al., 2006), for the period October 2010 to October 2014. The SNOWPACK model simulates the temporal evolution of the snow cover, given meteorological forcing conditions. It uses an explicit simulation of liquid water flow in snow, considering capillary suction as a function of snow properties, which enables to simulate ponding conditions inside the snowpack (Wever et al., 2014, 2015). The Alpine3D model performs a SNOWPACK simulation for each grid point in a two-dimensional grid, taking into account variable meteorological forcing due to terrain (elevation and aspect). We combine those simulations with records of wet snow avalanches that have been documented by the Swiss avalanche warning service for the same area, to assess the snowpack conditions in the release zones of the observed avalanches.

Avalanche dynamics models principally solve the mass and momentum balance in the avalanche using a terrain model and calculate, among others, flow thickness (perpendicular to slope) and velocity in the avalanche (Christen, Kowalski, & Bartelt, 2010; Mergili et al., 2017; Vera Valero et al., 2016). The RAMMS-Extended model has recently been extended with a temperature equation and phase change description as well as a friction dependent on water content to be able to simulate wet snow avalanche runout (Vera Valero et al., 2015). Using this model, we back-calculate the observed avalanches to evaluate whether the size of the recorded avalanches can be reproduced.

2. Data and Methods

2.1. Study Area

The studied area of Davos is located in an alpine environment in the Eastern Swiss Alps and covers approximately 460 km^2. The topography extends from 1,267 m to 3,218 m and is shaped by a major northeast to southwest valley, in which the town of Davos is located (see Figure 1). Three northwest to southeast oriented valleys branch off from the main valley, and the topography thereby spans a relatively complete range of slope aspects and elevations. Furthermore, avalanche prone slopes, defined as a slope angle of 30° or more, can also be found in a wide range of slope aspects and elevation.

The Davos area is considered an inner alpine region, indicating that it is relatively sheltered by large mountain ranges at all sides. This leads to a relatively shallow snowpack compared to other parts of Switzerland, with a typical maximum snow depth ranging from 180 to 290 cm. The shallow snowpack has been associated with an increased presence of persistent weak layers, such as depth hoar (Techel, Zweifel, & Winkler, 2015). However, while the snowpack in the region often contains such weaknesses, considerable variability can be noted between winters. For example, in 2012, a relatively deep and homogeneously layered snowpack resulted in many glide snow avalanches (Techel et al., 2013) not observed in the other years.

The winter in this part of the Alps can be separated into a midwinter season and a spring snow melt season (Wever et al., 2014). At high elevations, above 2,500 m, the snow cover typically starts to build in October/November and lasts until the end of June. During the midwinter season (December–February), the daily average temperature ranged from −23.7 to 4.2 °C at the Weissfluhjoch measurement site in the studied period. Accordingly, relatively little snow melt occurs in midwinter, except for the valley bottom or steep south facing slopes. Typically in March, the spring snow melt season starts, dominated by periods of melt which are regularly interrupted by colder periods with snowfall at times. Correspondingly, wet snow avalanche activity is mainly concentrated during the transition from the midwinter season to the spring snow melt season and is often related to instabilities formed by persistent weak layers (Baggi & Schweizer, 2009). Rainfall seldom occurs in the midwinter season and is mostly restricted to elevations below 2,000 m. The vast majority of rain-on-snow events, which can be a strong trigger for wet snow avalanches (Conway & Raymond, 1993), occurs during the spring snowmelt season (Würzer et al., 2016).

2.2. Data

To provide a full documentation of avalanche activity for the Davos area, the Swiss avalanche warning service — also based in Davos — records all reported avalanche activity. Avalanches are reported by a network of observers (e.g., ski patrol, mountain guides) and the public. In addition, the warning service surveys the area regularly in an attempt to provide a full documentation of avalanche activity, although some areas that are difficult or dangerous to access may not be visited regularly. Moreover, due to bad visibility or adverse weather conditions, avalanche activity can be missed or release dates may be uncertain. For the majority of events, release times are unknown.

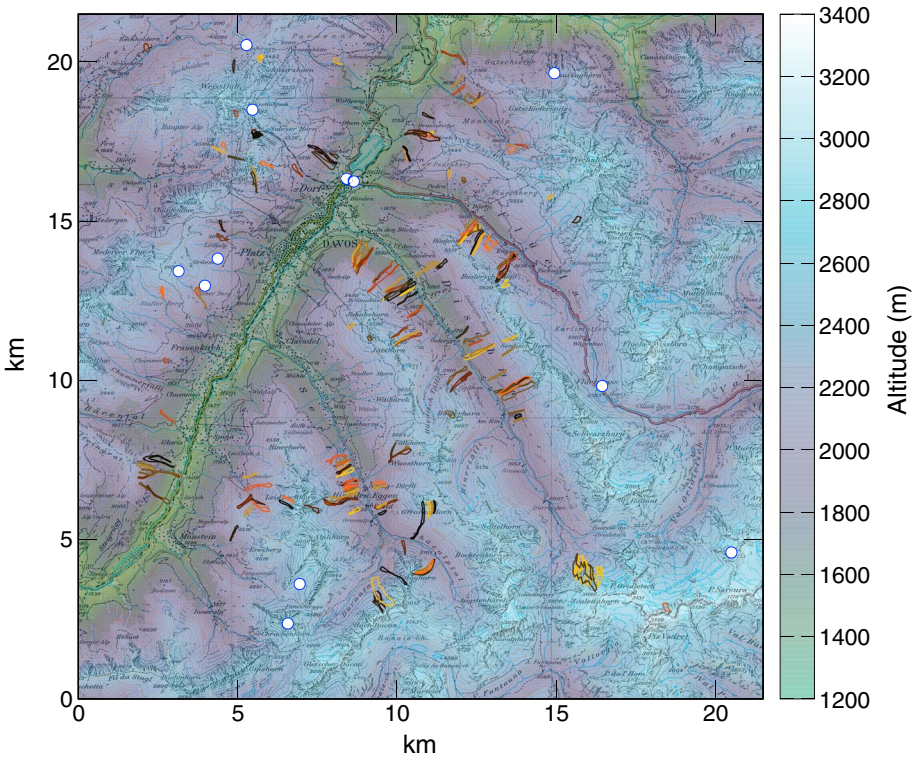

Figure 1. The digital elevation model of the simulation domain around Davos. The outline of all 169 avalanches for which avalanche dynamics calculations were performed are shown. White circles with blue outline denote the weather stations in the area used to drive the Alpine3D model. Map reproduced by permission of swisstopo (JA100118).

Avalanches are manually classified by wetness—as a dry snow or a wet snow avalanche (Dürr & Darms, 2016). This wetness estimate should refer to the wetness in the release zone. However, misclassifications are possible, particularly when the estimate is based on the avalanche debris (Bellaire et al., 2017). Avalanches classified as wet may be glide snow avalanches, loose snow, or wet slab avalanches. Additionally, a georeferenced outline of the avalanche is documented, containing both the release and the deposit area, but without separating between both. A comparison of mapped polygons with digital elevation model analysis has also revealed that the mapping of the polygons has inaccuracies regarding the exact positioning in the terrain, inherent to the method of using photos to manually map avalanches (Bühler et al., 2013).

For the period October 2010 to October 2014 (four winter seasons), a total of 1,615 avalanches classified as wet snow avalanches have been recorded for the Davos area. Many of the recorded avalanches are very small or small avalanches with path lengths up to 200 m and volumes up to 1,000 m^3 (Dürr & Darms, 2016). As the RAMMS-Extended model, which we use to simulate runout distances, is neither designed nor verified using very small and small avalanches, and to reduce the amount of data analysis and simulations, we selected only those 255 polygons whose projected surface area is larger than 0.0125 km^2. These avalanches are larger than the grid cell size we used for the Alpine3D model, which we consider to be important to have representative snowpack simulations in the release area. Following the definition of wet snow avalanches mentioned before, we consider the decisive criterion to classify an avalanche as wet when the snow in the release area is wet. In 169 of those 255 polygons, the simulations showed a volumetric liquid water content (LWC) in the release area of more than 2% in at least one snow layer below the upper 10 cm of the snowpack. Only those polygons are selected to perform avalanche dynamics calculations. Figure 1 shows the area of Davos, and the subset of 169 avalanche polygons for which avalanche dynamics simulations were carried out.

2.3. Methods

Note that we follow Fierz et al. (2009) for definitions and color schemes for snow profiles. We refer to slope perpendicular measures as *thickness*, and to vertical measures as *depth*.

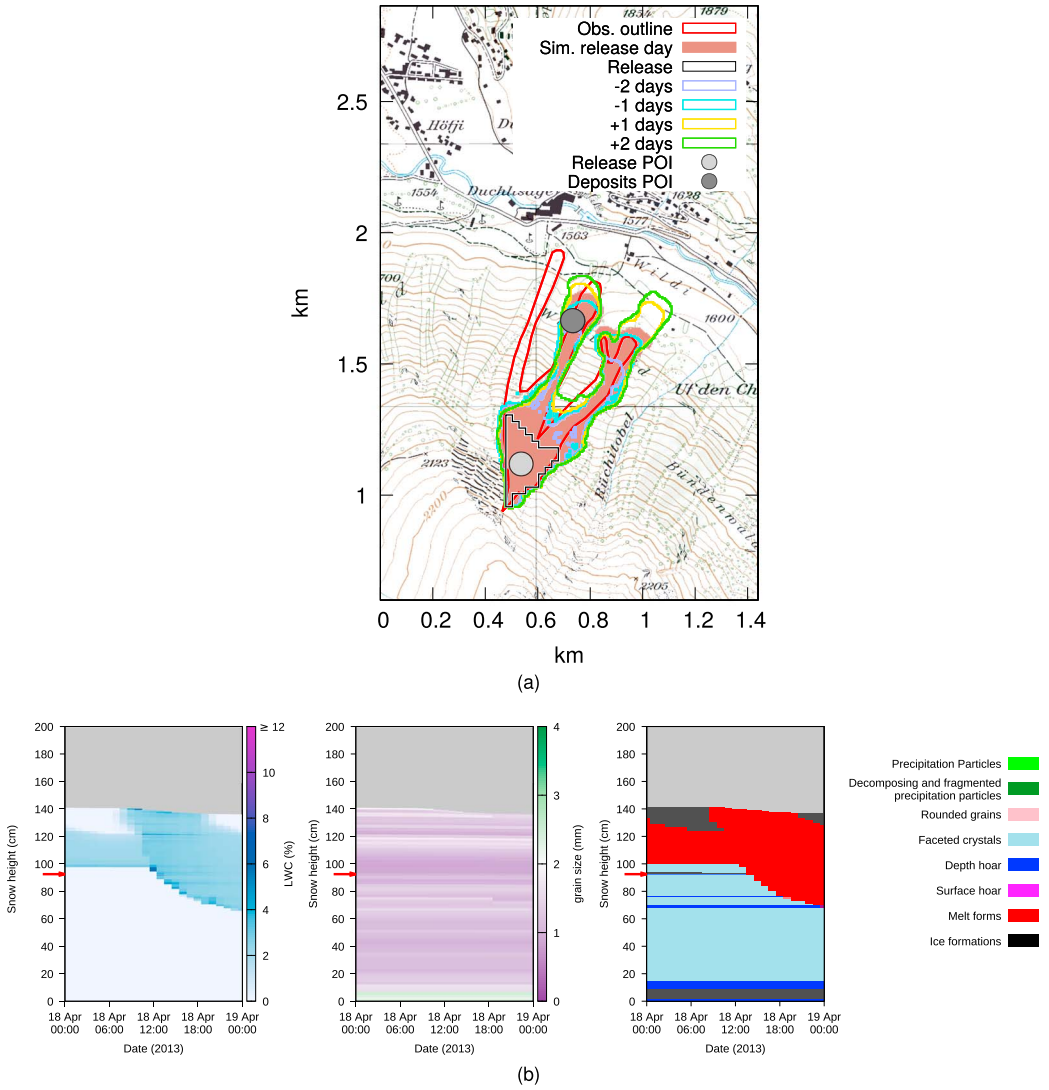

Figure 2. An example of (a) an avalanche as documented by the Swiss avalanche warning service [event ID: 198759248] and (b) the corresponding simulated snow cover for the date the avalanche occurred, for LWC, grain size, and grain type, respectively. In Figure 2a the observed and simulated avalanche polygon is shown as a red and a brown-filled polygon, respectively. The outline of the avalanche simulation for 2 days and 1 day prior to, as well as 1 day and 2 days after the release day are shown as violet, blue, yellow, and green polygons, respectively. The black polygon delineates the determined release area. The light and dark grey dots denote the points of interest (POI) for the release and deposit area, respectively, for obtaining detailed Alpine3D model output. In Figure 2b the red arrow denotes the release depth determined via the maximum local LWC. Reported release time for this avalanche is approximately 15:00. Map reproduced by permission of swisstopo (JA100118).

2.3.1. Data Preparation

The data set of avalanche activity contains polygons of all terrain affected by the avalanche, without separating in release, transit, and deposit area. Figures 2a and 3a show examples of polygon outlines projected on a Swiss topographic map. Note that these examples correspond to the *Brämabüel 2013* and *Drusatscha* case studies presented in Vera Valero et al. (2018). Release areas were assumed to correspond to the 25% of the pixels with the highest elevation inside the polygons, determined from the 25 m digital elevation model of the area, provided by Swisstopo (2018a). Similarly, the deposit areas were defined as the 25% lowest pixels. In Alpine3D, special points of interest are set in the middle of the release and deposit areas (indicated by the large dots in Figures 2a and 3a), such that a full, detailed snow profile could be extracted (examples in Figures 2b and 3b). This information is used to analyze snowpack properties in the avalanche release zone and to provide the initial and boundary conditions for the RAMMS-Extended model.

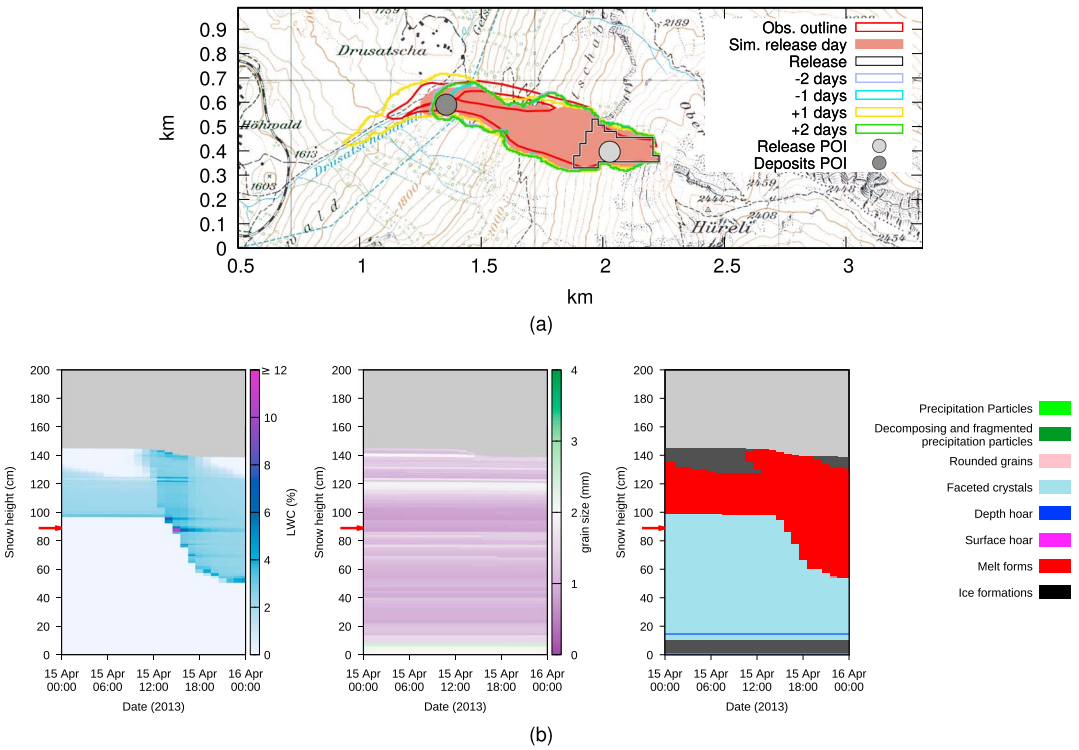

Figure 3. An example of (a) an avalanche as documented by the Swiss avalanche warning service [event ID: 198759173] and (b) the corresponding simulated snow cover for the date the avalanche occurred, for LWC, grain size, and grain type, respectively. See Figure 2 caption for explanation. Reported release time for this avalanche is approximately 17:00. Map reproduced by permission of swisstopo (JA100118).

Note that some avalanche polygons overlap, indicating that the avalanche paths were active multiple times. In most cases, these concern unrelated events in different years. However, in 2011, 2012, and 2013, release areas overlapped in surface area by 1.7%, 1.8%, and 3.3%, respectively. The full avalanche polygons share an area of 3.9%, 8.7%, and 8.4%, for 2011, 2012, and 2013, respectively. In 2014, all avalanche polygons are fully separated. The effect of multiple events in the same snow season in the same avalanche path on the snowpack stratigraphy and the avalanche flow is not considered in this study.

2.3.2. Alpine3D Model Setup

The simulation setup for the Alpine3D model and the simulated area surrounding Davos is virtually identical to the one presented in Vögeli et al. (2016) and Wever et al. (2017). The model domain is 21.5 × 21.5 km^2 in size, consisting of 215 × 215 grid cells with a grid cell spacing of 100 m. For each grid point, the elevation, slope angle, and aspect are determined from the digital elevation model. Meteorological forcing conditions for each grid point are determined using various interpolation techniques applied to measurements from several meteorological stations in the Davos area (see Figure 1), using the MeteoIO preprocessing library (Bavay & Egger, 2014). Precipitation over the area was determined by applying the elevation gradient from two heated rain gauges at 1,590 m (Davos) and 2,536 m (Weissfluhjoch, WSL Institute for Snow and Avalanche Research SLF, 2015), respectively. Temperature, relative humidity, and wind speed were interpolated from 11 weather stations inside and outside the model domain using inverse distance weighting of residues that remain after applying the lapse rate determined from the available stations to the digital elevation model. The separation of precipitation in rain or snow is done for each pixel individually using a fixed air temperature threshold of 1.2 °C. To distribute the incoming shortwave radiation over the grid, measurements from the MeteoSwiss station Weissfluhjoch-Gipfel (2,691 m) near Weissfluhjoch is split in a diffuse and a direct part. The diffuse part is distributed homogeneously over the model domain, whereas the direct part is distributed taking into account slope angle and aspect. The longwave radiation is also measured at the Weissfluhjoch-Gipfel and is interpolated over the model domain, considering grid point elevation, air temperature, and relative humidity.

In contrast to Wever et al. (2017), water flow in snow was described here by Richards equation (Wever et al., 2014) using the geometric mean for hydraulic conductivity at the interface nodes, as in Wever, Vera Valero, and Fierz (2016). Richards equation enables the simulation of water accumulating on microstructural transitions (Wever et al., 2015), although it increases computing times considerably. Using 36 CPU cores from a HPC system consisting of a total of 32 compute nodes with two 6-core AMD Opteron 2439 2.8 GHz processors per compute node, the computations took up to 10 days of wall clock time for the snow rich year 2012. The long computation times partly resulted from the large amounts of model output requested for this study, which was written to network drives.

For the center points of both the release and the deposit areas, simulated snow profiles from the model were stored at an hourly time resolution, containing vertical profiles of, among other variables, snow density, LWC (θ) and snow temperature. For the release date, these profiles were analyzed for the maximum local LWC (θ_{max}) inside the snowpack (Wever, Vera Valero, & Fierz, 2016). In the examples (Figures 2b and 3b), θ_{max} is indicated by a red arrow. We refer to the depth below the surface of θ_{max} as ponding depth. The time the daily maximum θ_{max} was reached was chosen as release time. The fracture depth is then assumed to correspond to the ponding depth. This assumption was found to provide very good agreement for a few avalanches where release depths were derived from drone imagery or terrestrial laser scans (Vera Valero et al., 2018). We calculated the average density of the snowpack above the fracture depth, forming the slab, as well as the average temperature and average LWC in the slab, from the simulated snow profile. In addition, we determined the percolation depth as the lowest layer interface where the upper layer had a LWC above 2%, whereas the lower layer had a LWC below 2%. Furthermore, we analyzed whether a layer consisting of depth hoar as primary grain type was first reached by water and at which depth below the surface this layer can be found. Only the depth hoar layer closest to the snow surface to get wet was considered.

2.3.3. RAMMS-Extended Model Setup

For all 169 release areas with θ_{max} exceeding 2% on the release day, avalanche dynamics simulations were performed using the RAMMS-Extended model (Vera Valero et al., 2016). The polygon containing the upper 25% of the pixels inside the observed avalanche polygon was set as the release area (see example in Figures 2a and 3a). We compare the release areas resulting from this procedure with the ones shown in the online supplement to Vera Valero et al. (2018) Figures S4 and S5 for *Brämabüel 2013* and *Drusatscha* cases, respectively. We find that for the *Brämabüel 2013* case (Figure 2), the release area in Vera Valero et al. (2018) corresponds to around the upper 10% of the pixels inside the polygon, whereas for the *Drusatscha* case (Figure 3) this is around 30%. This comparison suggests that the 25% selection criterion is acceptable as a suitable first-order approximation of the release area for commonly occurring avalanches, although the actual release area is highly uncertain.

For release depth, average slab density, snow temperature, and LWC, the results from the corresponding Alpine3D points were used. In the RAMMS-Extended model, the erosion layer properties were set equal to the properties in the release area for the elevation of the release area. From the ratio of simulated snow depth in the Alpine3D point between the release and deposit area, the gradient in the layer depth of snow available for possible erosion was derived. The median gradient in this layer depth available for erosion for the 169 cases was found to be 0.7 m/km of elevation, congruent with earlier reported values of 0.8 m/km (Fischer et al., 2015). From the release and deposition snowpack simulations, linear gradients in snow temperature were derived and also provided to the RAMMS-Extended model.

The avalanche dynamics simulations solve the force balance of an avalanche, which principally depends on the momentum of moving mass (released and eroded) and the friction on the terrain. The RAMMS-Extended model has three parameters that are considered specific to the avalanche path or dependent on snowpack properties, governing either the mass in motion or the friction (Vera Valero et al., 2018).

The erodibility defines the rate at which the snow cover along the avalanche path is being eroded (Christen, Kowalski, & Bartelt, 2010; Vera Valero et al., 2016). Wet snow avalanches often resemble plug-type flow (e.g., Sovilla et al., 2008), which is associated with higher erodability. Furthermore, the erodibility tends to be dependent on the depth of the erosion layer (Vera Valero et al., 2018). We implement these result here by setting the erodibility to 0.8 in case the snow thickness is less than 80 cm and 0.6 otherwise. Higher erodibility values mean that more snow is entrained in the avalanche path, which tends to increase the avalanche runout.

Terrain and snowpack properties can modify the shear stress in the avalanche, which is related to the fluidization process. Two parameters, the cohesion (Pa) and a coefficient α are considered to depend on snowpack properties and terrain, respectively. The cohesion describes how snow particles stick together (Bartelt et al., 2015). Typically, the cohesion is considered to range from 50 Pa for very dry, cold snow avalanches to 150 Pa for wet snow avalanches (Bartelt et al., 2015). Here we simulate wet snow avalanches only and the cohesion was consequently set to 150 Pa for each avalanche path. The coefficient α describes fluidization as a function of the terrain (Vera Valero et al., 2016). Typically, strong transitions in the terrain, such as cliffs, gullies, and rock outcrops increase the fluidization process in the avalanche, which can be described by a value of around 0.08 for α. The terrain in the area of Davos is relatively homogeneous (i.e., open faces without abrupt changes in slope angle), for which a value of 0.06 is assumed. These values are based on expert knowledge acquired in previous studies (Vera Valero et al., 2016, 2018). Within the context of this study, a calibration experiment with the RAMMS-Extended model is not feasible due to the high computational demand.

All simulations were performed on a 5-m resolution digital elevation model, resized from a 2-m resolution digital elevation model provided by Swisstopo (2018b). Previous studies found the optimal grid cell size for average size avalanches to vary between 2 and 5 m, as a balance between the smoothing effect of the snow cover on the terrain as well as representing small terrain features (Veitinger et al., 2014; Vera Valero et al., 2018) and optimizing computation times. A single simulation for one avalanche path took on average 12 min. In addition to the simulations for the release day, simulations for the 2 days preceding and the 2 days following the release day were performed. The five simulations per avalanche path for 169 avalanche paths, required about 170 hr CPU time on a typical personal computer.

The moving mass stopping criterion was used, which means that the simulation is stopped when the momentum is less than 5% of the maximum momentum during the simulation (Christen, Kowalski, & Bartelt, 2010). This stopping criterion is typically used with RAMMS but may result in different stopping times for different simulations even in the same avalanche path. This may influence the final simulation pattern, especially for small avalanches, where slow creeping flow behavior can be expected (see, e.g., Teich et al., 2014).

Several methods exist to validate avalanche dynamics model output (Mergili et al., 2017; Teich et al., 2014; Vera Valero et al., 2018). We focus here on maximum flow thickness, rather than pressure, to validate the model output. The documented avalanche polygons are drawn based on visual observations of the avalanche debris and track followed by the avalanche, which supposedly corresponds well to the maximum flow thickness. From the simulations, the area where the maximum flow thickness exceeded 5 cm was considered the area covered by the avalanche. Runout distances are sensitive to this threshold, as was tested for using the avalanche simulations in this study. Using a 2-cm or 8-cm threshold, compared to the 5-cm one, results on average in a 6.5% increase or 7.2% decrease in runout distance, respectively.

Runout distance is commonly analyzed (e.g., Fischer, 2013; Teich et al., 2014; Vera Valero et al., 2018) as well as inundated area (Mergili et al., 2017; Vera Valero et al., 2018). Runout distances were calculated by following the flowlines while searching for the intersection points with the maximum flow thickness field and the observed polygon, for the simulated and observed runout distance, respectively (see Vera Valero et al., 2018). We also compare the inundated area (i.e., the full area affected by the avalanche flow) from the maximum flow thickness in the simulations and the observed polygon using the Equitable Threat Score (ETS), similar to Vera Valero et al. (2018). The ETS evaluates the inundated area via a contingency table analysis, where the area is divided in four classes: an area only hit by the simulated avalanche, only hit by the observed avalanche polygon (i.e., included inside the polygon), or by both, or by neither. The ETS score summarizes these four areas by a score that is weighing hits or misses to the same extent. ETS is considered unbiased (Gandin & Murphy, 1992), which means that the score cannot be improved by consequently overpredicting or underpredicting the inundated area and that the score is also independent of the frequency of the hits (i.e., the avalanche size in our case). This makes ETS scores comparable between the different avalanche simulations concerning various avalanche sizes.

3. Results

3.1. Snowpack Characteristics in Wet Snow Avalanche Release Zones

We first analyze the simulated snow wetness in the avalanche release areas. Figure 4 shows the distributions of θ_{max} on the release day for the 169 selected avalanches, as well as the 2 days preceding and 2 days following the release day. On average, there is an increase in θ_{max}, peaking on the release day and slightly receding

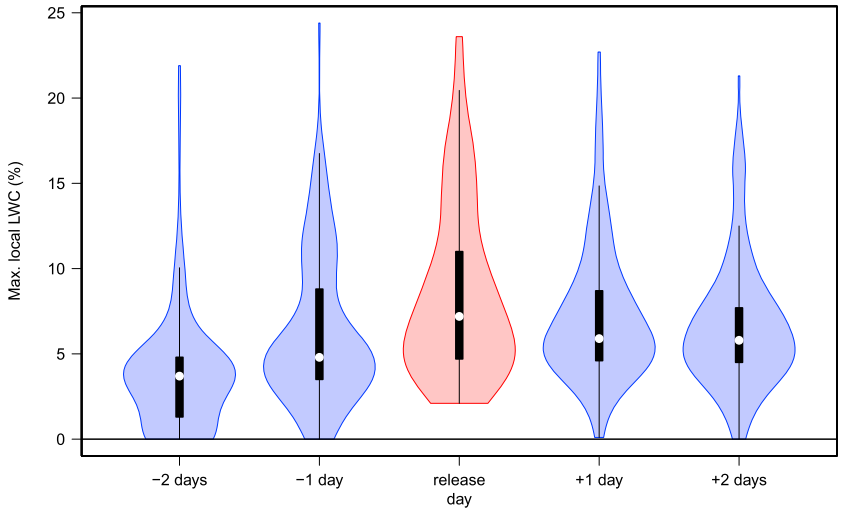

Figure 4. Distribution of maximum local LWC (θ_{max}) inside the release areas of all 169 avalanches with a maximum local LWC exceeding 2% on the release day, for the release day, and the four adjacent days, shown as violin plots (Hintze & Nelson, 1998). The violin plot combines a box plot (shown in black) with a symmetrically plotted rotated kernel density. The cutoff at 2% for the release day results from the selection procedure of avalanches, which required the simulations to indicate wet snow on the release day.

afterward. A two-sided Kolmogorov-Smirnov (KS) test showed that all distributions of θ_{max} differ significantly ($p < 0.001$) from the distribution on the release day. Similarly, the two-sided Wilcoxon test showed that the median value of the distribution on the release day is significantly different ($p < 0.001$) from the median values of the other days. As bulk LWC stays typically below 4% (Heilig et al., 2015), values of θ_{max} well over 5% indicate ponding on microstructural transitions. The large proportion of cases with θ_{max} exceeding 5% on days and in locations where wet snow avalanches released suggests that water ponding occurred.

The snowpack simulation for the example in Figure 2b shows a water accumulation at approximately 45-cm depth below the snow surface on a microstructural transition formed by a thin crust. On the day the avalanche released, deeper layers of the snowpack—consisting of facets and depth hoar—underwent wetting for the first time, while the upper layers—consisting of melt forms and a melt-freeze crust—had undergone wetting before. Note that the maximum water accumulation is reached at around 12:00, whereas the avalanche reportedly occurred at approximately 15:00. The example shown in Figure 3b shows ponding on a typical capillary barrier where fine grains can be found on top of coarse grains, although the grain type shows homogeneous layering. Here the maximum water accumulation can also be found earlier (around 14:00) than the avalanche reportedly occurred (approximately 17:00).

Figure 5a shows the temporal evolution of θ_{max} over all 169 release areas, relative to the day of release. Typically, the wet snow avalanche release happens during the first wetting phase: The snowpack is dry 10 days or more before the release (median 5 days). Following the onset of wetting, θ_{max} increases up to the day of the wet snow avalanche release. After the day of release, θ_{max} decreases again. This is congruent with the notion that capillary barriers are particularly creating high local LWC during the first wetting, as discussed in Wever, Vera Valero, and Fierz (2016). Once water flows over the capillary barrier, the increased hydraulic conductivity below the layer reduces the strength of the barrier. Additionally, wet snow metamorphism reduces the contrasting properties forming the capillary barrier.

Figure 5b shows the temporal evolution of the change in percolation depth (i.e., position of the meltwater front inside the snowpack). The day with observed avalanche activity is accompanied by a strong increase of almost 30 cm in percolation depth, not matched later in the season. The change in percolation depth for the release day is statistically significant compared to the day before and the day after (Wilcoxon test, $p < 0.001$). Note that negative values are related to the snow depth decreasing during the melt season, which effectively also decreases the percolation depth.

However, when considering the individual avalanche events, the highest θ_{max} within $\pm$10 days is found on the release day only in 26% of the cases, although in 72% of the cases, θ_{max} exceeded 5% on the release day.

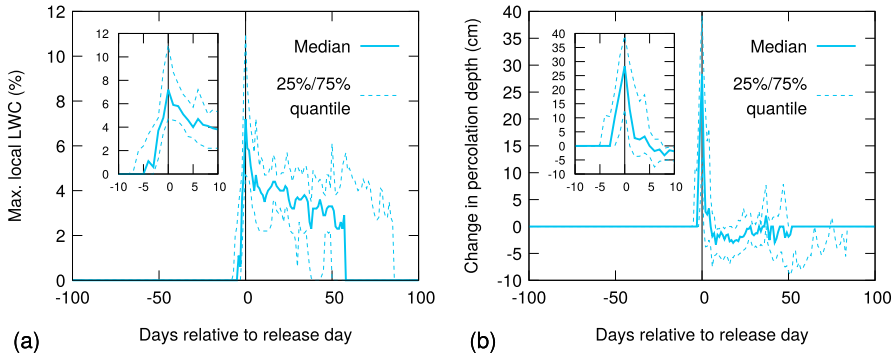

Figure 5. Distributions of (a) maximum local LWC (θ_{max}) and (b) change in percolation depth in the release areas of all 169 avalanches, centered around the release day (i.e., release day is set to 0, positive values on the *x* axis denote later days in the season). The inset shows the period between 10 days before the release day and 10 days after the release day.

In 20% of the 169 cases, the release day was the first day in the melt season on which θ_{max} exceeded 5%, and in 62% of the 169 cases, θ_{max} exceeded 5% for the first day in the melt season within a 5-day period centered around the release day. Similarly, the change in percolation depth is largest on the release day only in 30% of the release areas. This illustrates that predicting slope by slope is still challenging, as also shown by the large spread between the 25% and 75% quantiles shown in Figures 5a and 5b.

Figure 6 shows the depth below the snow surface where θ_{max} can be found on the release day, as well as the 2 days preceding and following the release day. The simulations show an increase of ponding depth during these days, indicating that water accumulations form on deeper layers on subsequent days. Note that the upper 10 cm of the snowpack is ignored, which results in a minimum slab depth of 10 cm on the release day. The median slab depth is found at 30 cm. In around 5% of the cases, the slab depth exceeds 1 m. The average released volume is 3,290 m^3.

Figure 6 also shows the depth of the melt water front, defined as the depth below the surface where the LWC drops below 2%. This measure shows a stronger increase than the depth of θ_{max}. The difference between both depths increases the most on the day of release, indicating that the melt water front progresses much deeper than where the largest water accumulations are found. Note that the difference between the position of the melt water front and θ_{max} is occasionally negative (i.e., the maximum local LWC is below the meltwater

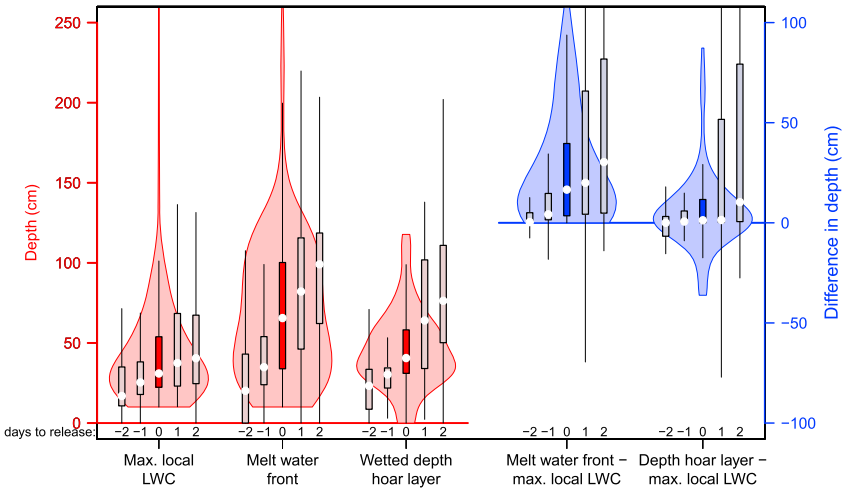

Figure 6. Violin plots of the depth below the snow surface of (i) the maximum local LWC (θ_{max}), (ii) the melt water front, and (iii) the depth hoar layer that got wet on the release day, shown on the left *y* axis in red. Violin plots for (iv) the difference of the depth between the melt water front and θ_{max}, and (v) between the depth of the depth hoar layer and θ_{max} are shown on the right *y* axis in blue. For the 2 days preceding and following the release day only box plots are shown in gray.

front). This counterintuitive result originates from the fact that θ_{max} is also defined when the LWC is generally below 2% throughout the snowpack, whereas the meltwater front is positioned at the snow surface in such cases. Furthermore, the top 10 cm is ignored when searching for θ_{max}, whereas it is not for the position of the meltwater front.

It is often reported that depth hoar layers that become wet for the first time loose strength rapidly, potentially leading to an avalanche release (e.g., Techel et al., 2011). Therefore, the depth of depth hoar layers becoming wet on the respective day is also shown in Figure 6. Up to and on the release day, the depth seems to regularly correspond closely with the depth where θ_{max} is found. The differences between both depths is also illustrated in Figure 6. The median of the differences is close to zero, suggesting that water accumulations are often simulated on top of layers with depth hoar.

3.2. Snow Wetness on Days with Multiple Avalanches

We now focus on the 6 days with most avalanches. Figure 7 shows the temporal evolution of θ_{max}, relative to the day of release. Here we analyze all the release areas of the avalanches regardless of the simulated wetness state. The 6 days cover 125 of the total of 255 avalanches. In all cases, the snowpack is on average at least partially wet. The median of θ_{max} exceeds 5% in five of the six cases. The avalanches in the shown events all occurred during the first wetting, as θ_{max} in the period before the release remains well below 4%. In two cases, the highest median of the 200-day period is found on the release day or, in the case of 1 March 2012, 1 day later.

Figure 8 shows the distribution of θ_{max} as a function of slope aspect and elevation for the same 6 days. These days are shown side by side based on the year in which they occurred. It appears that in 2012 and 2013, days which were among the 6 days with highest activity were consecutive, and in 2011 there was a 7-day time span in between. In all six cases, the wet snow avalanche cycle can be associated with a marked and rapid increase of the 0° isotherm to elevations exceeding 3,000 m. For illustrative purposes, all reported avalanche activity is shown, even the avalanches smaller than 0.0125 km^2 which were excluded from the analysis (small circles). In the supporting information, the two preceding and the two following days for each of those 6 days are shown.

For 1 April 2011 as well as 8 April 2011 (Figure 8, plots in upper row), the avalanche activity was concentrated first in E-NE and W-NW sectors, and 1 week later in the north sector (NW-N-E). This is supported by the wetness simulations, which show the highest values of θ_{max} inside these sectors. Both days were during a phase of increased ponding conditions (see Figures S1 and S2 in the supporting information). On 1 April 2011, the model seems to underestimate the wetting, as considerable wet snow avalanche activity occurs outside the band with θ_{max} exceeding 5%. For 8 April 2011 (Figure S2 in the supporting information), the expansion of the ponding conditions is most pronounced 1 day before the avalanche activity has been observed. The 2 days following 8 April 2011 exhibit quickly receding ponding conditions, congruent with no reported avalanche activity.

For both days, however, the south facing slopes still exhibit values of θ_{max} well over 5%, with only a few very small avalanches reported. Here it is of note that many of these slopes had already avalanched during a first wetting phase in March (Techel & Pielmeier, 2013). Furthermore, even though melt rates in the south facing slopes are presumably higher than in the sectors where most avalanche activity has been reported, the strength of present capillary barriers is apparently less such that less water accumulates on those barriers than in E-NE and W-NW facing slopes. As mentioned earlier, previous wetting, and wet snow metamorphism probably has partly homogenized the snowpack in south facing slopes.

The two consecutive days in 2013 (14 and 15 April 2013, Figure 8, middle row) show similar patterns: the avalanche activity is reported for slope aspects and elevations that are within bounds of the area with simulated snow wetness exceeding 5%, but the SE-S sector seems to only have activity from very small avalanches, in spite of simulated high θ_{max} inside the snowpack. As in the situation in 2011, a previous wetting period in March on southerly aspect start zones had already caused the release of mostly small wet snow avalanches (Techel, Stucki, et al., 2015). The supporting information Figures S5 and S6 show rapidly expanding ponding conditions on these 2 days, followed by a rapid decrease afterward, which is congruent with the temporal evolution of avalanche activity. These examples illustrate once more that just the presence of a water accumulation is not decisive and that particularly the first wetting causing water ponding inside the snowpack seems critical.

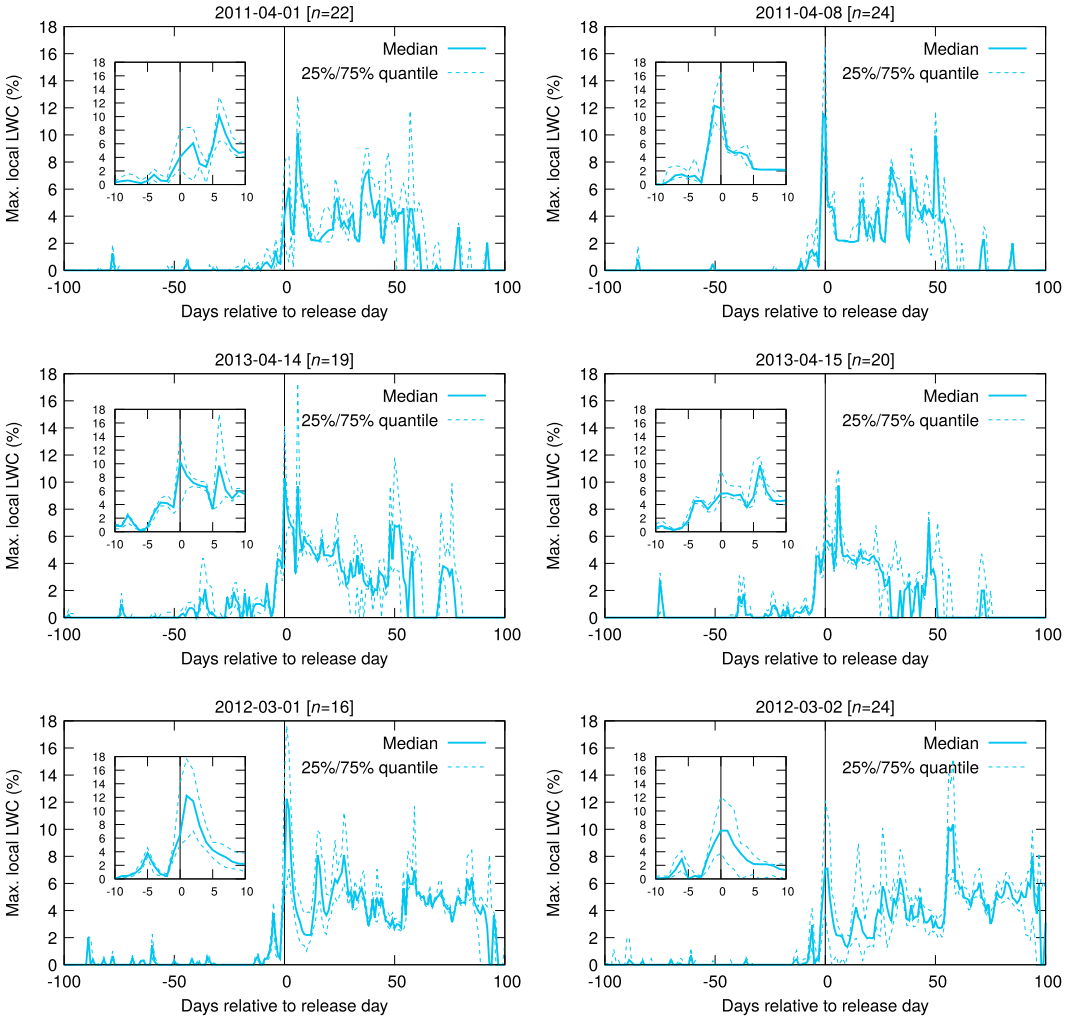

Figure 7. Distributions of maximum local LWC (θ_{max}) in the release areas of all avalanches larger than 0.0125 km^2 that occurred on a single day, for the 6 days with the largest number of avalanches, organized by year. The number of avalanches on the specific day (*n*) is shown inside the squared brackets. Further explanation is provided in the caption of Figure 5.

In contrast with 2011 and 2013, the situation in 2012 (1 and 2 March 2012, Figure 8, lower row) shows important wetting in south aspects (SE-SW), which expands to higher elevation as well as E and W aspects the following day. Initially, observed avalanche activity is fairly well restricted to this sector only but spreads to more aspects and elevations with continued wetting (2 March 2012: E-S-W). The beginning of March 2012 was the most intensive wet snow avalanche period of the winter with numerous wet snow and glide snow avalanches recorded (Techel et al., 2013). As shown in the supporting information Figures S3 and S4, the snowpack transitioned from dry to wet within a few days in the E-S-W sector and the avalanche activity is concentrated during this transition. Even though the 0° isotherm rapidly increased to around 3,000-m elevation, the north sector still remains dry. The situation in 2012 occurred earlier in the season than in the other years. We attribute the different wetness pattern in 2012 to a colder snowpack and lower incoming solar radiation combined with a more unfavorable incident angle in the north sector. The supporting information Figure S4 shows that the wetting did not expand further in the days following the avalanche cycle.

3.3. Avalanche Size and Runout

The RAMMS-Extended simulations were used to explore avalanche size and runout, resulting from the snowpack state as simulated by Alpine3D. Using the same parameters and keeping the size of the release area constant for each avalanche, simulations vary with respect to release mass (fracture depth and slab density) as well as snow temperature and LWC.

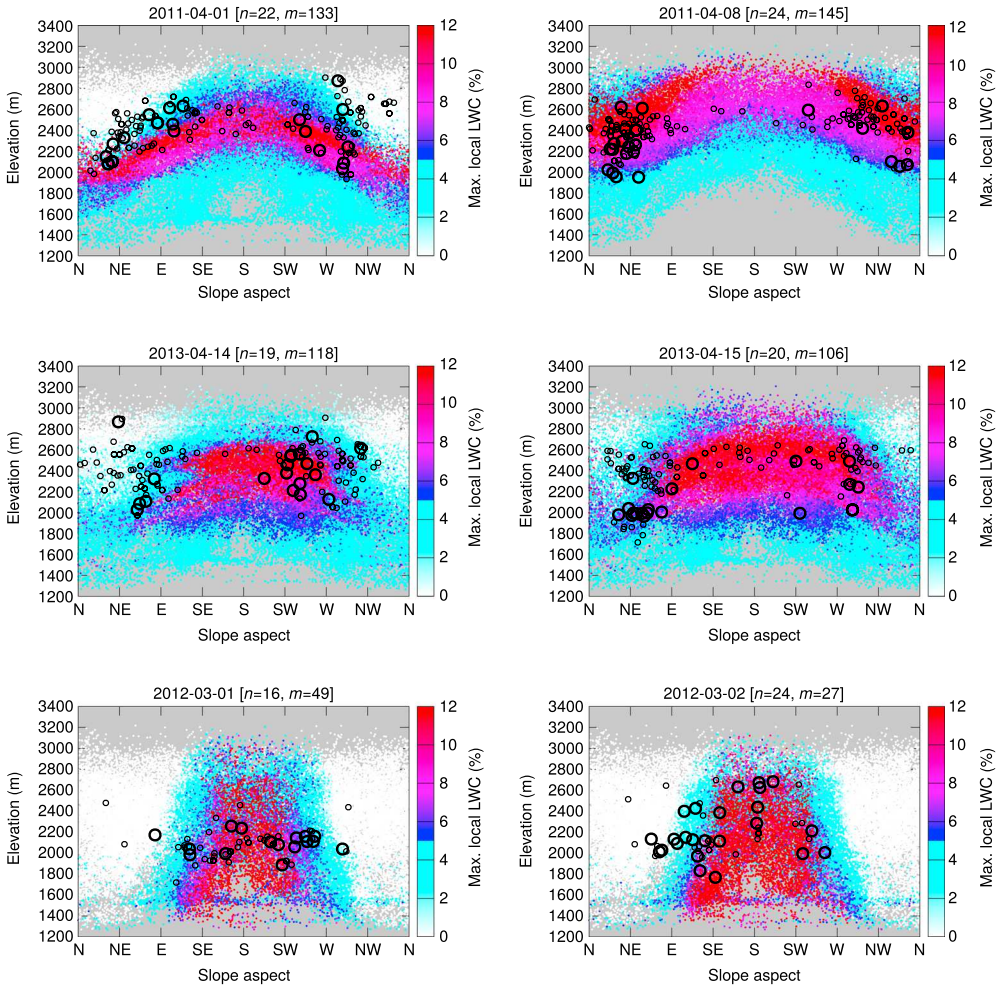

Figure 8. Slope aspect and elevation of all grid points inside the model domain with a snow depth exceeding 10 cm, colored according to the maximum local LWC (θ_{max}), for the 6 days with the largest number of avalanches, organized by year. The slope aspect and elevation of the release areas of reported avalanches are denoted by open black circles. Large circles represent the avalanches with a surface area larger than 0.0125 km^2, as selected for this study (number of avalanches denoted by *n*). Small circles represent all other avalanches reported (number of avalanches denoted by *m*).

The skill in reproducing the inundated area is verified using the ETS, where an ETS of 1 denotes a perfect simulation (i.e., the simulated inundated area perfectly matches the documented polygon from the observed avalanche), 0 or negative score denotes no skill. In addition, the runout distances were compared to the ones derived using the documented polygons from the observed avalanches. Here a negative absolute error or a relative error smaller than 1 in runout distance denotes an underestimated simulated runout distance compared to the documented observed avalanche and vice versa. Figures 9 and 10 show the ETS and both the absolute and relative error in runout distance, respectively, for the 169 simulated avalanches on the release day. For the other days (1 and 2 days before and after the release day, respectively), only avalanches where θ_{max} exceeds 2% in the snowpack in the release area for all 5 days are shown, which considers 116 avalanches. For the other 53 cases, the snowpack is dry at one or more of the two adjacent days, making it impossible to determine initial conditions for a wet snow avalanche simulation.

The highest ETS values are typically achieved on the release day. The 2 days prior to the release day show lower ETS values for the avalanche simulations. The 2 days following the release day show very similar ETS values, as in contrast with percolation depth, the depth of θ_{max} remains relatively comparable to the one on the release day (see Figure 6). Only the distribution of 2 days before the release day is significantly different (two-sided KS test, $p = 0.031$) from the one on the release day. Similarly, only the median ETS differs significantly between the 2 days before the release day and the release day (two-sided Wilcoxon test, $p = 0.006$).

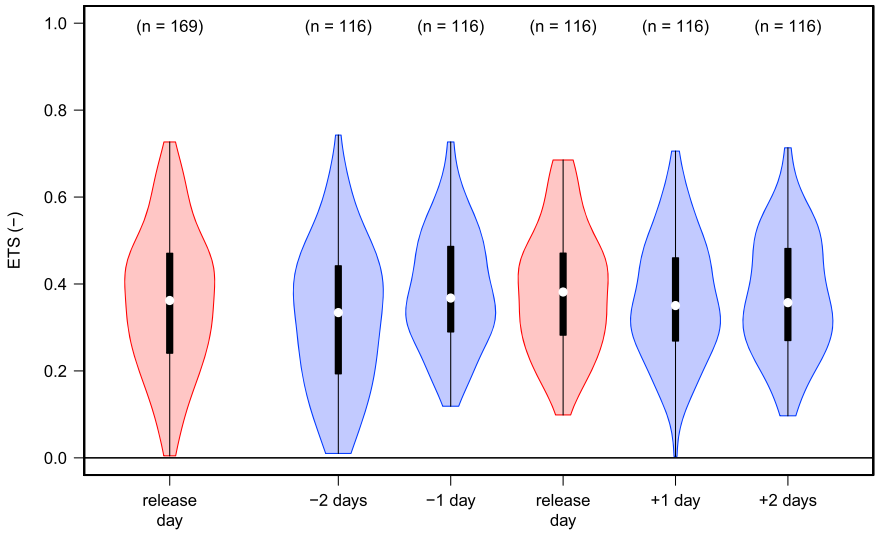

Figure 9. Equitable threat scores (ETS) for the avalanche dynamics calculations, shown as violin plots (Hintze & Nelson, 1998). Shown is the distribution for all considered avalanches on the release day, as well as the distributions for the release day and the four adjacent days for the release zones having over 2% LWC locally in the snowpack in all five consecutive days. A score of 1 denotes a perfect simulation, 0 or negative indicates no skill from the simulation.

The median error in absolute runout distance from the simulations is close to 0, but the spread is very large (Figure 10). Errors in runout distance of several hundred meters regularly occur. The median relative runout distance error is close to 1 and varies between 0.25 and 2, indicating a tendency to underestimate the runout distance. The large spread indicates that predictions for individual avalanche paths remain difficult, particularly without avalanche path specific calibration of the RAMMS-Extended model. However, averaging over avalanche paths seems to yield statistically significant results. The 2 days prior to the release day show a larger underestimation of the median runout distance, although only the comparison of the 2 days before the release with the release day is statistically significant at the 95% confidence level for both the distribution (two-sided KS test, $p < 0.001$) as well as the median (two-sided Wilcoxon test, $p < 0.001$). For the comparison of the 1 day before the release day with the release day, only the median tests significantly different (two-sided Wilcoxon test, $p = 0.012$), whereas the KS test for the distribution yields $p = 0.031$.

It may seem an unsatisfying result that only the RAMMS-Extended simulations between 2 days before the release day and the release day itself are statistically significantly different. However, it should be noted that the comparison only involves avalanche paths where the snowpack was considered at least partly wet in the release zone for all 5 days. This means that the cases where a dry snowpack is simulated, and consequently no wet snow avalanche is expected, are excluded.

There is no statistically significant correlation between the depth of the maximum local LWC and the runout distance derived from the observed polygons (Pearson $r = -0.03$, $p = 0.66$). In contrast, the correlation between observed and simulated runout distance is statistically significant (Pearson $r = 0.55$, $p \ll 0.001$), indicating that topography is a strong control on the runout and that avalanche dynamics models are capable of capturing the effect of an avalanche release given the terrain.

3.4. Case Studies

Two avalanches in our data set have been analyzed before in Vera Valero et al. (2018). For the example shown in Figure 2 (case *Brämabüel 2013*), the runout distance error is −54 m (observed: 966 m, simulated 912 m) and the ETS score is 0.51. The runout error is of opposite sign and slightly smaller in absolute value in this study than in Vera Valero et al. (2018). The ETS score is not comparable, as the ETS score in this study is concerning the full avalanche polygon, whereas Vera Valero et al. (2018) validates the deposit area only. The Alpine3D simulation provides a smaller release thickness (38 cm) in the release area compared to the one derived from the virtual slope concept with SNOWPACK (111 cm) in Vera Valero et al. (2018). The simulation for 2 days after the release day (green polygon in Figure 2) is performed using a fracture thickness of 83 cm. This mainly affects the runout distance of the right arm of the avalanche, which was not validated in Vera Valero et al. (2018).

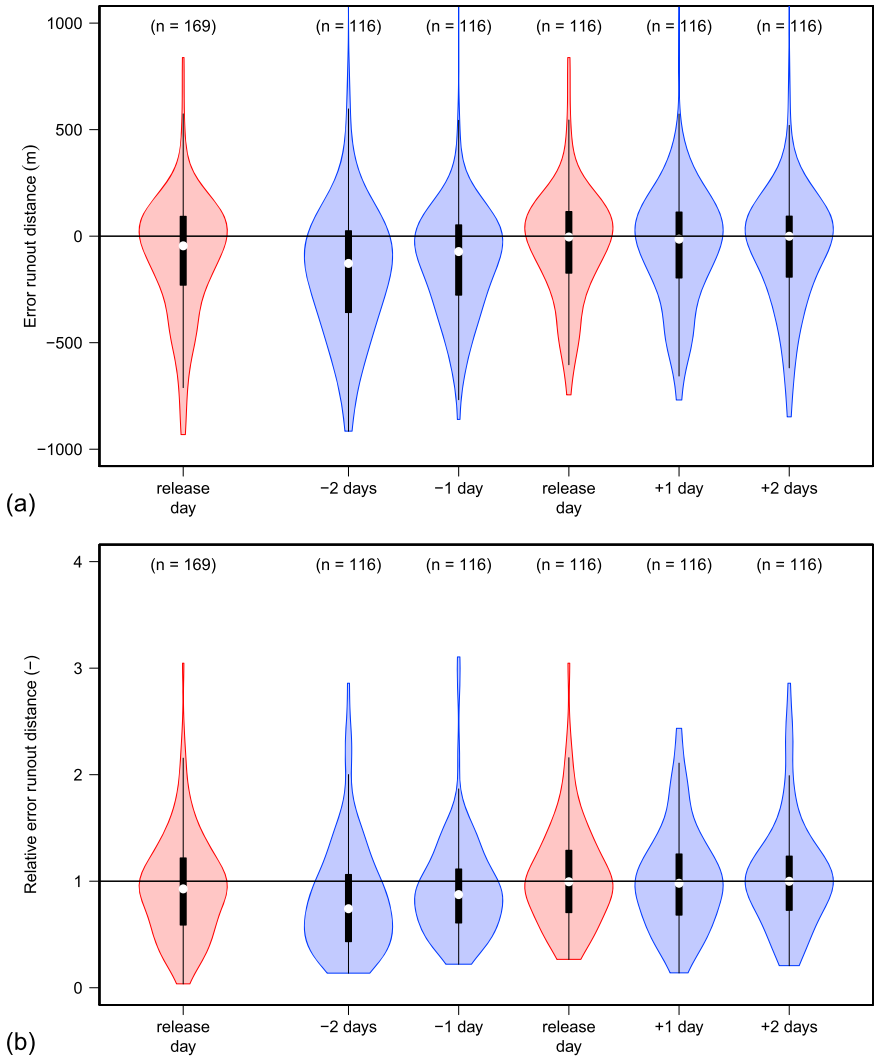

Figure 10. (a) Absolute and (b) relative error in runout distances from the avalanche dynamics calculations, shown as violin plots (Hintze & Nelson, 1998). Shown is the distribution for all considered avalanches on the release day, as well as the distributions for the release day and the four adjacent days for the release zones having a LWC locally exceeding 2% LWC in all five consecutive days. In (a), the *y* axis is restricted between −1,000 and +1,000 m.

The left arm is not reproduced by the depicted release area. Note that in Vera Valero et al. (2018), the about 3 times deeper release depth is compensated for by a smaller release area than determined here, resulting in a twice as large released volume in that study.

The *Drusatscha* example shown in Figure 3 shows a runout distance error of −177 m (observed: 1,257 m, simulated: 1,079 m) and an ETS score of 0.66. The Alpine3D simulation provides a smaller release thickness (44 cm) in the release area to the one derived from the virtual slope concept with SNOWPACK (54 cm) in Vera Valero et al. (2018). The smaller and shallower release area used here is compensated for by a higher value of erodibility, although the simulated avalanche still runs short. The fracture thickness at 1 day after the release day (yellow polygon in Figure 3) was positioned at 74 cm below the surface, which leads to an overestimation of runout. Similar to the *Brämabüel 2013* case, the deeper release depth and slightly larger release area in Vera Valero et al. (2018), results here also in a twice as large released volume in that study.

To illustrate the varying degrees of model and observational agreement, we now show the results for the event with the approximately median runout distance error, as well as the events corresponding to the approximately 10% (underestimated) and 90% (overestimated) quantiles. Figure 11 shows an example of a good agreement between simulated and observed runout, having the approximately median runout distance error

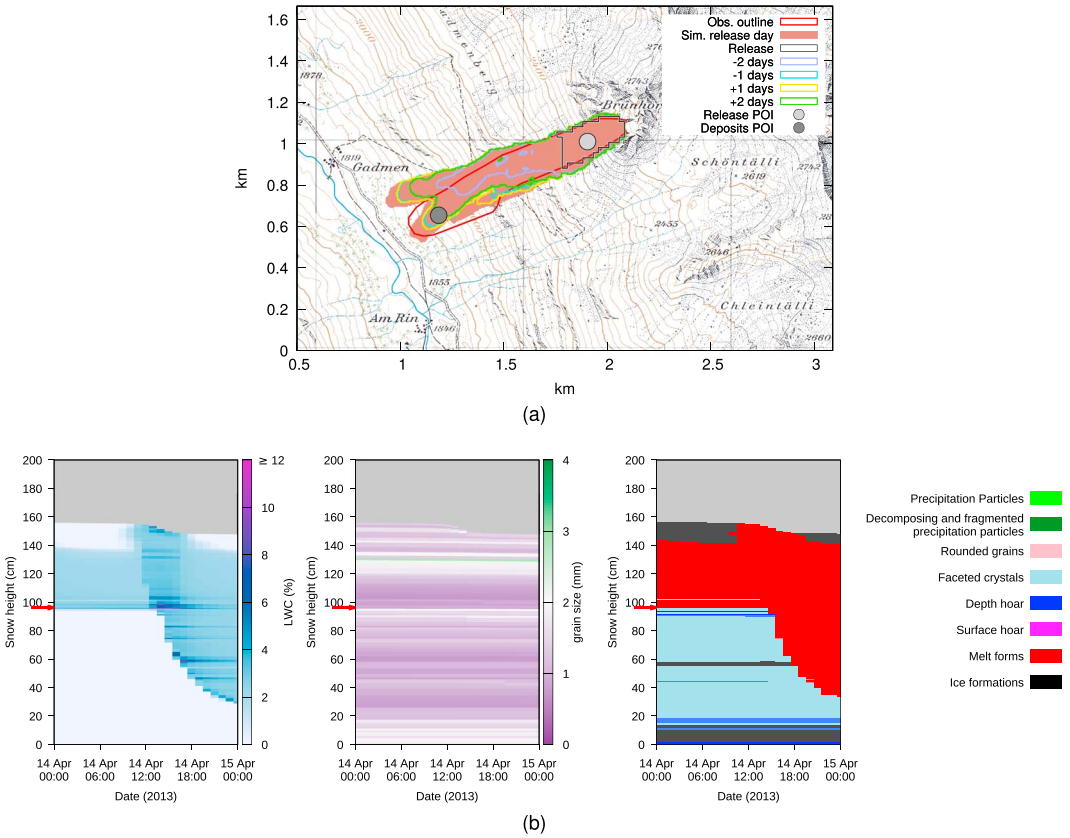

Figure 11. Simulation results for the event having the approximately median runout distance error of 31 m [event ID: 198758985], showing (a) the avalanche as documented by the Swiss avalanche warning service and the corresponding RAMMS-Extended simulations and (b) the corresponding simulated snow cover for the date the avalanche occurred, for LWC, grain size, and grain type, respectively. See Figure 2 caption for explanation. Map reproduced by permission of swisstopo (JA100118).

(ETS = 0.64, runout distance error: 31 m, simulated runout distance: 1,226 m, observed runout distance: 1,195 m). Two days prior to the release, the fracture thickness is estimated at 27 cm, resulting in a clearly underestimated runout distance. During the following days, water percolated deeper, and reached a layer of around 55-cm depth below the surface (see Figure 11b), corresponding to a fracture thickness of 44 cm. There ponding occurred on a layer with coarser grains and thin layers with depth hoar. Taking this depth as release depth yields a good correspondence with the observed avalanche. The days after the release day yield similar correspondence in the avalanche simulation, but the runout is slightly shorter. This may be due to the fact that the release depth decreases due to snow melt, when the same layer keeps on causing ponding conditions.

Figure 12 shows a strong underestimation of the runout distance error at the approximately 10% quantile (ETS=0.18, runout distance error: −630 m, simulated runout distance: 349 m, observed runout distance: 979 m). For the release day, as well as the 2 days prior and following the release day, simulations are covering a more or less similar area, much smaller than the observed one. The fracture thicknesses vary from 11 to 20 cm. On the release day, ponding occurs around 20 cm below the surface, while water has already percolated deeper. It can be imagined that a release at deeper layers where ponding conditions occur could create a better agreement with observed runout. However, the layer at 20 cm depth is causing the strongest ponding and is therefore chosen as release depth. The transition at 80 cm in grain size is not causing strong ponding, probably due to higher density, but a release at this layer could also be imagined.

Figure 13 shows a strong overestimation of the runout distance at the approximately 90% quantile (ETS = 0.28, runout distance error: 216 m, simulated runout distance: 532 m, observed runout distance: 316 m). Here the simulation 2 days prior to the release day, with a release thickness of 9 cm shows a very small avalanche, suggesting an underestimation of the release depth. The simulation 1 day after the release day, with a release

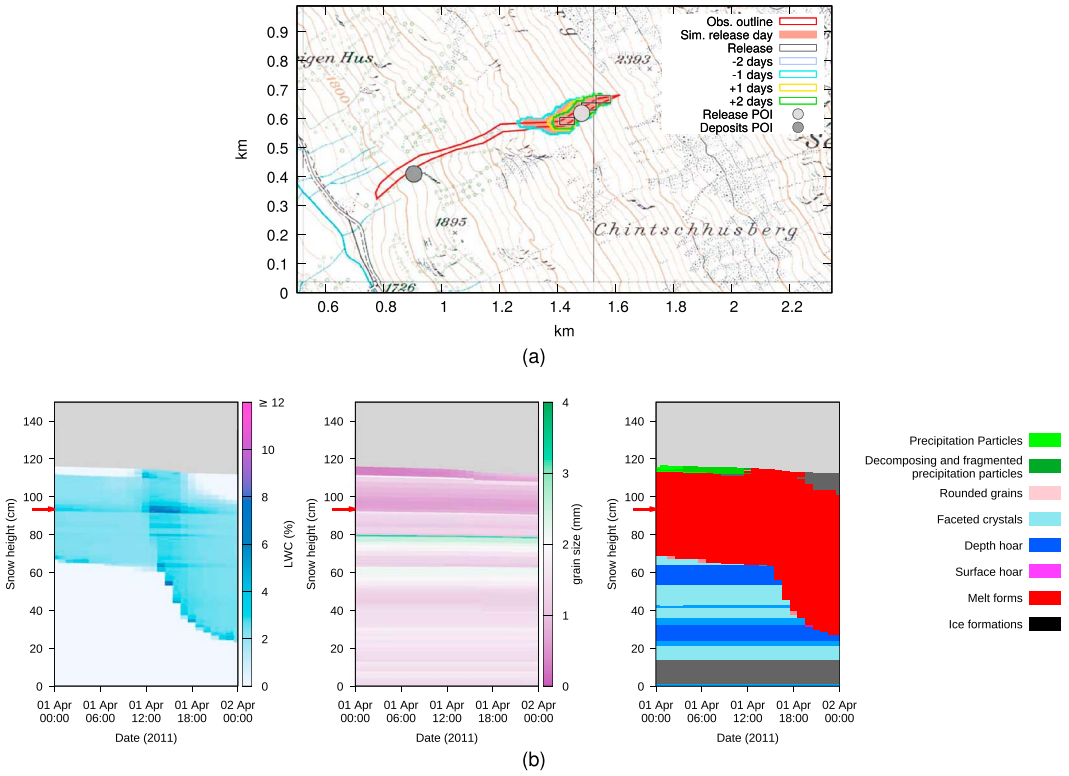

Figure 12. Simulation results for the event having the approximately lower 10% error in runout distance of −630 m [event ID: 1605650], showing (a) the avalanche as documented by the Swiss avalanche warning service and the corresponding RAMMS-Extended simulations and (b) the corresponding simulated snow cover for the date the avalanche occurred, for LWC, grain size, and grain type, respectively. See Figure 2 caption for explanation. Map reproduced by permission of swisstopo (JA100118).

thickness of 11 cm shows a larger avalanche, but still running too short. The simulations for 1 day before and 2 days after are very similar, resulting from a very similar release thickness of 14 and 15 cm, respectively. The deepest release occurs on the release day, at approximately 50 cm depth (release thickness: 44 cm).

4. Discussion

4.1. Snowpack Conditions

For 169 of 255 observed avalanches, the distributed snowpack simulations identified the presence of liquid water inside the snowpack. However, for 86 observed avalanches that were classified as wet, the snow cover simulations did not show snow layers with more than 2% LWC below the uppermost 10 cm. This discrepancy does not necessarily indicate a failure of the model to reproduce the state of the snowpack. Potential explanations may also be related to the presence of glide snow avalanches in the data set (i.e., winter 2011–2012), misclassifications for avalanches that released as a dry snow avalanche and entrained wet snow along the path, resulting in wet snow deposits, and data entry errors. A timely verification of the snowpack conditions in the release zone of wet snow avalanches is often not possible as these areas are usually difficult or dangerous to access. Furthermore, as, for example, indicated by the pronounced advance of the wetting front on avalanche days (Figure 6), changes in wet snow are rapid such that manual observations will rarely capture the right place and time and additionally, the spatial variability can be considerable (Techel & Pielmeier, 2011). Hence, we can neither truly verify the simulated snowpack conditions nor the wetness classification of the reported avalanches. Despite this drawback, we argue that due to the rapid evolution of snow wetness in time and space, distributed numerical snowpack modeling may provide a suitable solution to continuously monitor the evolution of the snowpack during phases of wetting.

For the days with multiple avalanches, we found that the simulations often show a rapid transition from dry to wet snow around the days with wet snow avalanche activity. These results are in agreement with field observations indicating that the period of the first wetting of the snowpack is one of the most critical periods

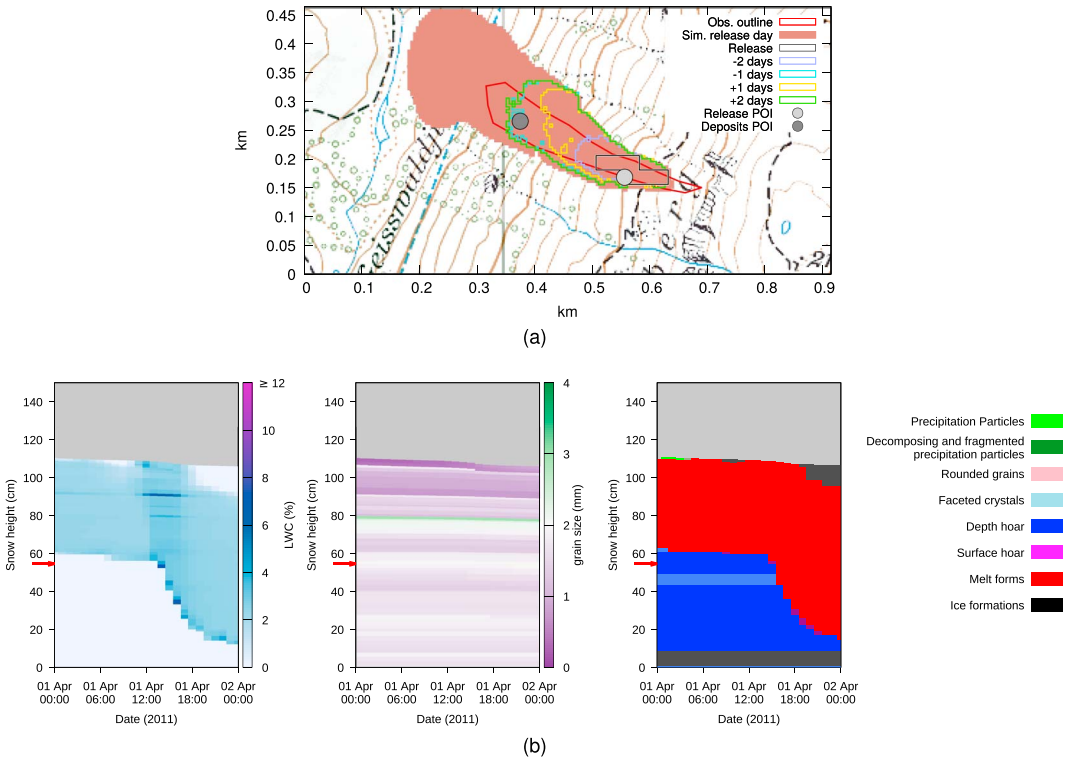

Figure 13. Simulation results for the event having the approximately upper 90% error in runout distance of 216 m [event ID: 1605584], showing (a) the avalanche as documented by the Swiss avalanche warning service and the corresponding RAMMS-Extended simulations and (b) the corresponding simulated snow cover for the date the avalanche occurred, for LWC, grain size, and grain type, respectively. See Figure 2 caption for explanation. Map reproduced by permission of swisstopo (JA100118).

(Baggi & Schweizer, 2009; Mitterer & Schweizer, 2013). Note that prior knowledge of the date and location of occurred avalanches is exploited in this study and we did not address the false alarm rate, that is, how often the first wetting and the occurrence of capillary barriers with θ_{max} exceeding 5% is not accompanied by wet snow avalanche activity.

The timing of water percolation in the snowpack corresponded to avalanche activity with varying degrees of success. Several factors influence the simulated water percolation. An accurate simulation of the energy balance is necessary, which requires high-quality measurements of incoming shortwave and longwave radiation, as well as several weather stations to capture the varying meteorological conditions in the area. Small-scale terrain features may cause a strong heterogeneity in the local energy balance, which is not captured by the strong terrain smoothing resulting from the 100-m grid cell spacing in the Alpine3D model. Furthermore, microclimates in slopes are not represented by the meteorological stations, which are all located in flat areas. The effect of measurement errors and the contribution of uncertainties in meteorological input variables to model simulation errors using Alpine3D has been assessed in Schlögl et al. (2016). That study focused on snow water equivalent, which is influenced by both precipitation input and snow melt, and estimated an influence of measurement and interpolation uncertainties to be up to 30%.

Water percolation timing and slab depths also depend on the local snow depth distribution. The general snow cover distribution is well captured using the two rain gauges, as shown by Vögeli et al. (2016), although a comparison with remote sensing snow data showed that local deviations can be significant as a result of snow redistribution by wind. Additionally, more accurate descriptions of water flow in snow accounting for preferential flow (e.g., Wever, Würzer, et al., 2016), may improve the timing of arrival of liquid water on microstructural transitions deep inside the snowpack. This is particularly true for first wetting, and low-density snow (Würzer et al., 2017).

Rainfall is considered an important factor contributing to wet snow avalanche activity, as it is not only accompanied by strong melting of the snowpack and an increase of LWC, but also because of the added mass (Conway & Raymond, 1993). We used a fixed air temperature threshold of 1.2 °C to separate between rain or snowfall. Although this threshold value provides an accurate partitioning on long time scales, it may be highly variable for a particular event (Harpold et al., 2017). This means that we can easily miss or falsely predict rainfall on an event basis. However, wet snow avalanche activity combined with rainfall seems rare in our data set: only for 9 out of the 169 avalanches considered in this study, rainfall contributed more than 1% of the daily precipitation sum on the day of the event, based on the 1.2 °C threshold.

4.2. Wet Snow Avalanche Release

The principle we used in this study is that water accumulating on microstructural transitions corresponds to the failure layer depth in case of wet snow avalanches. Indeed, the presence of capillary barriers has been linked to wet snow avalanche activity (Baggi & Schweizer, 2009). Wet slab fracture line profiles showed the failure within or at the layer interface of a soft layer consisting of faceted or depth hoar grains below a fully moist, melt forms layer with smaller grains (Techel & Pielmeier, 2010). Fierz and Föhn (1994) report the release of wet snow avalanches above ice layers, for which water ponding on the ice layer seemed to have caused the release. Techel and Pielmeier (2009) noted, however, that standard snowpack stability tests did not identify layers with high water content due to ponding as the failure plane. The authors suggested that either those tests are not suitable for this type of failure, or saturated layers are not relevant failure planes, but are only indicating the presence of microstructural transitions and weak layers.

Laboratory studies have found that ponding on microstructural transitions may create layers of a few centimeter depth inside the snowpack with LWC values up to 30%–40% (Avanzi et al., 2016). Snowpack models, among them SNOWPACK, were able to reproduce these results (Avanzi et al., 2016; Hirashima et al., 2017), when considering grain size and density-dependent water retention curves (Yamaguchi et al., 2012). Note that in sloped terrain, one can expect lower values of LWC due to the occurrence of lateral flow, even though the reduced gravity force perpendicular to the slope in sloped terrain would enhance the water ponding effect (Leroux & Pomeroy, 2017).

Similar to the results from Wever, Vera Valero, and Fierz (2016), the simulations presented here confirm that reaching a threshold around 4% to 6% LWC within the snowpack for a first time seems to adequately capture periods with wet snow avalanche activity. This is congruent with strength experiments on wet snow. Initially, low amounts of LWC are considered to increase the shear strength due to additional capillary forces (e.g., Reiweger et al., 2016) and consequently, Brun and Rey (1987), for example, found no decrease of shear strength up to 6% LWC. In the funicular regime (LWC exceeding 8%; Colbeck, 1973; Fierz et al., 2009), snow is generally considered to have low shear strength. In contrast, other studies have shown a quick reduction of shear strength at low LWC (around 2%) in layers with facets and depth hoar (Reiweger et al., 2016; Techel et al., 2011; Yamanoi & Endo, 2002). Those layers typically consist of coarse grains and have relatively low density compared to adjacent layers. In the experimentally determined water retention curve by Yamaguchi et al. (2012), both low snow density as well as coarse grains exhibit low capillary suction due to large capillaries. Consequently, high values of LWC are not often reached. These low values seem nevertheless to be sufficient to cause a strength reduction (Techel et al., 2011), and an increase in crack propagation propensity (Reiweger et al., 2016). The collapse of such weaknesses in the snowpack was proposed as an important trigger mechanism for wet snow avalanches by Techel and Pielmeier (2009) and Techel et al. (2011), while Reardon and Lundy (2004) observed large wet snow avalanche cycles, in particular, when such weak layers were present at the base of the snowpack. Ultimately, we cannot identify the exact release mechanisms. However, our results suggest that water accumulations often occurred above persistent weak layers—like depth hoar—that may fail during wetting. It is likely too simplistic to only focus on the accumulation with the highest LWC, without considering the strength of the snow.

The approach of looking at water accumulations inside the snowpack is representing the case of wet slab avalanches. However, wet glide snow avalanches or wet loose snow release avalanches are also considered wet snow avalanches (McClung & Schaerer, 2006). Hence, we do not span the full range of wet snow avalanches in this study. Regarding glide snow avalanches, assessing the LWC at the base of the snowpack and the soil is important (Ceaglio et al., 2017; McClung & Clarke, 1987). In our simulations, we neglect the presence of vegetation, while the soil is initialized with a coarse material to absorb almost all water draining from the snowpack. Furthermore, the hydraulic conductivity of the soil is not reduced when soil freezing occurs,

which in reality may occur (e.g., Azmatch et al., 2012). In the current simulation setup, we are not able to correctly assess water accumulating at the snow-soil interface resulting from a reduced permeability of the soil in case of soil freezing or the influence of vegetation on snowpack runoff. Our model setup is therefore not suitable to adequately analyze cases with glide snow avalanches.

Wet loose snow avalanches can be triggered by snow from rocks, trees, or bushes, which warm more efficiently than the snowpack. In such cases, the growth of the loose snow release toward a wet snow avalanche can still be influenced by liquid water in the snowpack, as well as the presence of gliding surfaces inside the snowpack, which can also act as capillary barriers above which water accumulations form (Vera Valero et al., 2016). Even though the exact release mechanism for loose snow releases is not adequately captured in the Alpine3D model, the resulting depth of mass entrainment may be correctly predicted based on the presence of ponding water inside the snowpack (Vera Valero et al., 2016).

4.3. Avalanche Dynamics Simulations

The concept of water accumulating on microstructural transitions and locally exceeding 5% as an indicator for wet snow avalanche activity would gain importance if the depth at which this occurs bears any correspondence with the actual fracture depth, which we assumed in this study. Unfortunately, it is notoriously difficult to estimate fracture depths from a distance without visiting the release area or using measurement techniques such as drone photogrammetry, or laser scanning. Reliable validation data for the fracture depth is therefore generally not available. Vera Valero et al. (2018) show for a few examples of well-documented avalanches a good correspondence between simulated ponding depth and measured fracture depth.

On the one hand, we could not find a statistically significant correlation between release depth and observed avalanche runout distance. On the other hand, the avalanche dynamics simulations shown for the case studies exhibited a strong relationship of simulated runout with fracture depth. This has been noted in earlier studies (e.g., Barbolini et al., 2000; Bartelt et al., 1999; Vera Valero et al., 2018). The contrasting result suggests that predicting wet snow avalanche activity regarding snowpack conditions favorable for a release as well as the consequences of a release, cannot be achieved by information about the snowpack stability alone. In addition to the fracture depth, the topography places a strong control on avalanche runout, which can be described by avalanche dynamics modeling.

Similar to our conclusion that maximum local LWC and changes in percolation depth show a strong relationship with avalanche activity when analyzed over an ensemble of release areas, the avalanche size resulting from the ponding depth show a relationship with observed avalanche size only when analyzing it over an ensemble. The results indicate that predictions for individual avalanche paths remain challenging but that the combination of Alpine3D and RAMMS-Extended captures regional snowpack characteristics and resulting avalanche size. This suggests cautiously that the temporal evolution of the water percolation and the depth at which water accumulations formed during the periods with avalanche activity is, on average, adequately simulated.

However, substantial errors in runout distance and inundated area for individual avalanche paths were regularly found. This can be attributed to the propagation of the variability found in the results of water percolation in the snowpack simulations for the individual release areas to the avalanche simulations. Simulation errors in the RAMMS-Extended simulations add to the uncertainty from the snowpack simulations for determining the release depth, which results in high variability in the runout distances and inundated area. The three parameters that are considered dependent of avalanche path and snowpack characteristics would likely allow to improve the simulations for individual avalanche paths (Fischer et al., 2015), but the sensitivity to the fracture depth will remain. This has been illustrated by Vera Valero et al. (2018) by changing the fracture depth for well-studied and calibrated avalanche paths, which lead to an avalanche path-dependent sensitivity to runout distance. That study also showed a dependence of snow temperature and wetness on runout, but given the lack of verification for release depths in this study, we estimate that dependence to fall within the uncertainties caused by the other factors.

Determining the correct release area is one of the most important factors in obtaining a correct avalanche simulation. Algorithms have been developed to determine potential release areas (Bühler et al., 2013; Maggioni & Gruber, 2003; Veitinger et al., 2016). Generally, it is very difficult, however, to predict fracture propagation distances and thus to determine the final release area. In this study, we used the knowledge of where avalanches occurred and what the approximate cross-slope size of the avalanche

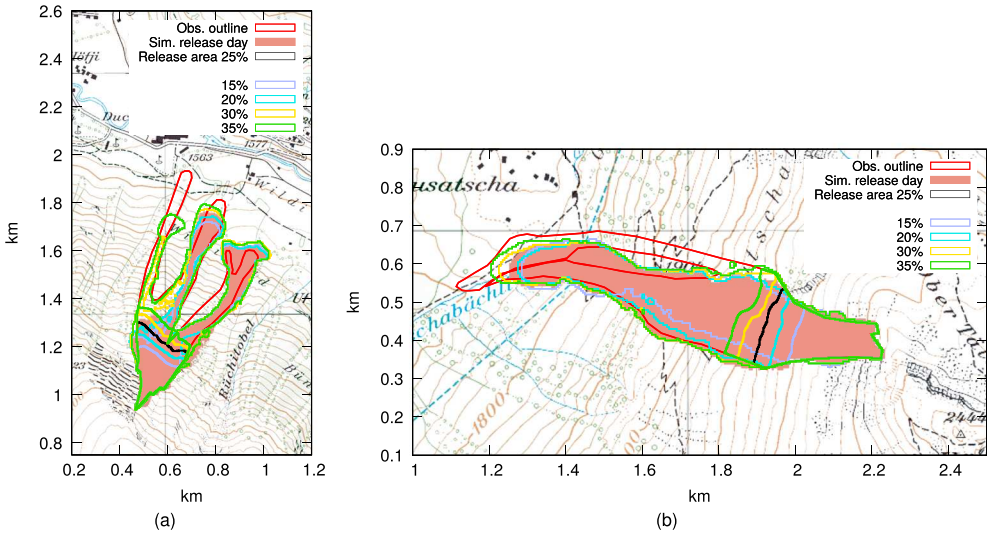

Figure 14. Simulation results for the two example events (a) *Brämabüel 2013* [event ID: 198759248] and (b) *Drusatscha* [event ID: 198759173], with varying definitions of the release area. The black release area corresponds to the definition of 25% highest area of the documented polygon (shown in red), as used throughout this study, and the brown area to the simulated inundated area. The other colors correspond to a release area and resulting simulation for a definition of release area consisting of 15%, 20%, 30%, and 35% highest area of the documented polygon. Maps reproduced by permission of swisstopo (JA100118).

was. This assists the avalanche dynamics simulations considerably. However, for small avalanches, misplacements of the observed avalanche polygons in the digital elevation model (Bühler et al., 2013), may also occasionally result in poor performance of the RAMMS-Extended model to reproduce inundated area and runout distance.

Additionally, it is unlikely that our approach to assume that the upper 25% of terrain touched by an avalanche forms the release area is appropriate for all terrain and all avalanche sizes. The 12 case studies shown in the online supplement to Vera Valero et al. (2018) show a clear variation in relative size of the release area to the total avalanche size. For the two example cases, *Brämabüel 2013* and *Drusatscha*, we performed a sensitivity study by varying the release area to be 15%, 20%, 30%, and 35% of the documented polygon, in addition to the 25% criterion used throughout this study. Figure 14 shows that the variability caused by varying the release area over this range is around 80 m for both cases. This is considerably less than the variability found by the varying fracture depths resulting from taking snowpack properties on the 5 days centered around the release day (see Figures 2a and 3a), which is 329 m and 524 m for the *Brämabüel 2013* and *Drusatscha* case, respectively.

The reason for the small sensitivity of release area size to the avalanche runout is that by extending the release area downslope in the avalanche path, the larger release area is compensated for by smaller possible erosion. The growth index, defined as the ratio of deposited over released mass, increases from 1.3 to 1.7 when decreasing the release area from 35% to 15% for the *Brämabüel 2013* case, and from 1.7 to 2.7 for the *Drusatscha* case, demonstrating the relationship between release area size and erosion. Previous studies have also shown the relative higher importance of fracture depth over release area in avalanche simulations (e.g., Barbolini et al., 2000; Christen, Bartelt, & Kowalski, 2010). The differences in the sensitivity of the growth index to the release area size between the two cases also illustrate the controlling behavior of the terrain on the avalanche flow and erosion. Note that the discussion above only holds for models that explicitly account for erosion, but not for Voellmy-Salm type models (Sovilla & Bartelt, 2002).

Some of the simulations tend to overestimate the width of the avalanches (see, e.g., Figures 12 and 13), suggesting an overestimation of the lateral spreading of mass. When avalanche are strongly confined by terrain features, the runout tends to increase, as suggested by the example in Figure 12. Consequently, lateral spreading of the mass may result in an underestimated runout distance by the model. This particularly holds when the lateral spreading is caused by a misplacement of the documented polygon in the digital elevation model, resulting in different flow behavior or a too coarse simulation resolution. The overestimation of the

width of the release area as a result of using a 25-m digital elevation model to determine the release area will also introduce lateral spreading. However, this is not expected to markedly influence the runout distance, as an overestimation of the release area width will also overestimate the released mass.

Finally, the map in Figure 1 shows several avalanche paths frequented multiple times in the data set. Their shape is similar and this suggests that it may be possible to construct typical release areas for frequently active avalanche paths based on historical records. This has the potential of using the model chain in this study for wet snow avalanche activity prediction, by simulating well-known avalanche paths in an area. This could more reliably verify the relationship between the simulated water percolation and the avalanche release.

5. Conclusion

We performed distributed, detailed snowpack simulations using the Alpine3D model for an area of ~460 km^2 around Davos in the Eastern Swiss Alps, for the four winter seasons 2010–2011 until 2013–2014. Using a grid cell spacing of 100 m, the snowpack simulations were forced by interpolated meteorological data from weather stations, taking into account local slope angle, aspect, and elevation. The snowpack was simulated by the SNOWPACK model within the Alpine3D model, using Richards equation for liquid water flow. Based on available records of avalanche activity, including georeferenced polygons of the area covered by the avalanche, detailed output was extracted from the simulations for the areas where wet snow avalanches occurred. From 255 selected avalanches after excluding the very small ones, simulations for 169 avalanches showed at least 2% LWC locally inside the snowpack in the release area. The others showed dry snow, possibly related to the fact that the database does not separate between glide snow and wet snow avalanches, but possibly also due to avalanche-type misclassifications in the database or uncertainties in the model and measured meteorological input data.

Generally, wet snow avalanches happen during the first wetting of the snowpack, as is very well reproduced in the simulations. Owing to a careful model setup driven by high-quality meteorological data, the timing of the wetting and liquid water accumulating on microstructural transitions, causing LWC to exceed 5% locally in the snowpack, is on average accurate within ±1 day. Often, these microstructural transitions are formed by depth hoar layers. Days with wet snow avalanche activity are also characterized by a strong increase in percolation depth of the melt water front in the release areas. However, the results also showed that for individual avalanche paths, simulating the correct conditions remains challenging. In less than 30% of the avalanches, the maximum local LWC and increase in percolation depth was highest on the day the avalanche has been observed within a ±10 day time span.

Using the assumption that the depth of the maximum local LWC can be considered the release depth of the avalanche, avalanche dynamics calculations were performed for 169 avalanches using the RAMMS-Extended model. Initial and boundary snowpack properties were provided by the SNOWPACK simulations. Results showed that on average, runout distances were well simulated. For avalanches where the snow in the release area was at least partly wet during the five consecutive days centered around the release day, the area affected by the avalanches and runout distances were best simulated taking the simulated snowpack state at the release day, instead of 2 days before. The 1 day preceding and the 2 days following the release day showed a very similar model performance (i.e., not statistically significantly different from the release day). This is congruent with the ±1 day accuracy found for maximum local LWC. The spread in results is relatively large, indicating that the model chain is in many cases not able to provide accurate predictions for individual avalanche paths. The results showed that the fracture depth plays a key role in the simulated runout distances. The uncertainty in simulated water percolation for individual avalanche paths thereby propagates to avalanche dynamics simulations. However, fracture depth itself did not correlate with runout distance. First, this illustrates that an assessment of avalanche activity in terms of release probabilities and avalanche size cannot be achieved by only characterizing the snowpack state. Second, similar to the distributed snowpack simulations of water percolation, the avalanche dynamics models seem suitable to link snowpack conditions to avalanche size, when analyzed as an ensemble. It cautiously confirms that ponding depths, and thus fracture depths, are on average adequately simulated.

The results from the distributed snowpack simulations as well as the avalanche dynamics simulations were found to provide useful information for a regional evaluation (i.e., with respect to elevation bands and slope aspects) of wet snow avalanche activity. Here, we exploited our prior knowledge of days and locations where avalanche activity has been observed, and we did not address the issue of false alarms.

However, we can imagine that for a known area with good historical records of avalanche activity, typical avalanche paths can be selected, with typical release areas. The coupling of both models could then be used for predictions of regional wet snow avalanche activity based on these selected avalanche paths.

Acknowledgments
We thank everyone who reported avalanche activity, which enabled to create a unique and detailed database. We also thank Andreas Stoffel for extracting and preparing the wet snow avalanche records from the database and Charles Fierz for useful comments on a previous version of the manuscript. We acknowledge the three anonymous reviewers, as well as the Associate Editor for providing constructive comments that helped to improve the manuscript. N.W. was supported by the Swiss National Science Foundation (SNSF), grant 172299. The wet snow avalanche activity data are available via https://doi.org/10.16904/envidat.39 (Swiss Avalanche Warning Service, 2018). The SNOWPACK, Alpine3D, and the MeteoIO preprocessing library are available under a LPGLv3 license under http://models.slf.ch. The model versions used here correspond to revision 367 (alpine3d/trunk) for Alpine3D, revision 1038 (snowpack/branches/dev) for SNOWPACK, and revision 1738 (meteoio/trunk) for MeteoIO. The RAMMS-Extended model can be requested via http://ramms.slf.ch. For the geospatial data processing, the open source GDAL library version 2.1.0 was used (GDAL Development Team, 2016) and statistical analysis (including the creation of the violin plots) was performed using the open source software R (R Core Team, 2015), version 3.2.3. The Alpine3D and RAMMS-Extended model setup and simulations can be accessed via https://doi.org/10.5281/zenodo.1283522. Meteorological data from the Weissfluhjoch measurement site can be accessed via https://doi.org/10.16904/1. Precipitation data for the Davos station were kindly provided by MeteoSwiss and can be requested via https://gate.meteoswiss.ch/idaweb. The automatic weather station data from the other stations in the area of Davos used to run the simulations can be requested via the SLF data service: https://www.slf.ch/en/services-and-products/data-and-monitoring/slf-data-service.html. The 2-m digital elevation model for the Davos area used in this study is the swisstopo swissALTI3D product, which can be requested via https://shop.swisstopo.admin.ch/en/products/height_models/alti3D.

References

Avanzi, F., Hirashima, H., Yamaguchi, S., Katsushima, T., & De Michele, C. (2016). Observations of capillary barriers and preferential flow in layered snow during cold laboratory experiments. *Cryosphere*, *10*(5), 2013–2026. https://doi.org/10.5194/tc-10-2013-2016

Azmatch, T. F., Sego, D. C., Arenson, L. U., & Biggar, K. W. (2012). Using soil freezing characteristic curve to estimate the hydraulic conductivity function of partially frozen soils. *Cold Regions Science and Technology*, *83–84*, 103–109. https://doi.org/10.1016/j.coldregions.2012.07.002

Baggi, S., & Schweizer, J. (2009). Characteristics of wet-snow avalanche activity: 20 years of observations from a high alpine valley (Dischma, Switzerland). *Natural Hazards*, *50*(1), 97–108. https://doi.org/10.1007/s11069-008-9322-7

Barbolini, M., Gruber, U., Keylock, C., Naaim, M., & Savi, F. (2000). Application of statistical and hydraulic-continuum dense-snow avalanche models to five real European sites. *Cold Regions Science and Technology*, *31*(2), 133–149. https://doi.org/10.1016/S0165-232X(00)00008-2

Bartelt, P., Salm, B., & Gruber, U. (1999). Calculating dense-snow avalanche runout using a Voellmy-fluid model with active/passive longitudinal straining. *Journal of Glaciology*, *45*(150), 242–254. https://doi.org/10.3189/S002214300000174X

Bartelt, P., Valero, C. V., Feistl, T., Christen, M., Bhler, Y., & Buser, O. (2015). Modelling cohesion in snow avalanche flow. *Journal of Glaciology*, *61*(229), 837–850. https://doi.org/10.3189/2015JoG14J126

Bavay, M., & Egger, T. (2014). MeteoIO 2.4.2: a preprocessing library for meteorological data. *Geoscientific Model Development*, *7*(6), 3135–3151. https://doi.org/10.5194/gmd-7-3135-2014

Bellaire, S., van Herwijnen, A., Mitterer, C., & Schweizer, J. (2017). On forecasting wet-snow avalanche activity using simulated snow cover data. *Cold Regions Science and Technology*, *144*, 28–38. https://doi.org/10.1016/j.coldregions.2017.09.013

Brun, E., & Rey, L. (1987). Field study on snow mechanical properties with special regard to liquid water content. In *Avalanche formation, movement and effects, Proceedings of the Davos Symposium, September 1986*, IAHS, Wallingford, Oxfordshire, U.K., publ. no. 162. pp. 183–193.

Bühler, Y., Kumar, S., Veitinger, J., Christen, M., Stoffel, A., & Snehmani, S. (2013). Automated identification of potential snow avalanche release areas based on digital elevation models. *Natural Hazards and Earth System Sciences*, *13*(5), 1321–1335. https://doi.org/10.5194/nhess-13-1321-2013

Ceaglio, E., Mitterer, C., Maggioni, M., Ferraris, S., Segor, V., & Freppaz, M. (2017). The role of soil volumetric liquid water content during snow gliding processes. *Cold Regions Science and Technology*, *136*, 17–29. https://doi.org/10.1016/j.coldregions.2017.01.007

Christen, M., Bartelt, P., & Kowalski, J. (2010). Back calculation of the In den Arelen avalanche with RAMMS: Interpretation of model results. *Annals Glaciology*, *51*(54), 161–168. https://doi.org/10.3189/172756410791386553

Christen, M., Kowalski, J., & Bartelt, P. (2010). RAMMS: Numerical simulation of dense snow avalanches in three-dimensional terrain. *Cold Regions Science and Technology*, *63*(1), 1–14. https://doi.org/10.1016/j.coldregions.2010.04.005

Colbeck, S. (1973). Theory of Metamorphism of Wet Snow (*CRREL report*): U.S. Army Cold Regions Research and Engineering Laboratory.

Conway, H., & Raymond, C. F. (1993). Snow stability during rain. *Journal of Glaciology*, *39*(133), 635–642.

Durand, Y., Giraud, G., Brun, E., Mérindol, L., & Martin, E. (1999). A computer-based system simulating snowpack structures as a tool for regional avalanche forecasting. *Journal of Glaciology*, *45*(151), 469–484.

Dürr, L., & Darms, G. (2016). *SLF-Beobachterhandbuch (Observation guidelines)*. Davos: WSL Institut for Snow and Avalanche Research SLF.

Feistl, T., Bebi, P., Christen, M., Margreth, S., Diefenbach, L., & Bartelt, P. (2015). Forest damage and snow avalanche flow regime. *Natural Hazards and Earth System Sciences*, *15*(6), 1275–1288. https://doi.org/10.5194/nhess-15-1275-2015

Fierz, C., Armstrong, R., Durand, Y., Etchevers, P., Greene, E., McClung, D., et al. (2009). The International Classification for Seasonal Snow on the Ground (ICSSG). Tech. rep., IHP-VII Technical Documents in Hydrology No. 83, IACS Contribution No. 1, UNESCO-IHP, Paris.

Fierz, C., & Föhn, P. (1994). Long-term observations of the water content of an alpine snowpack. In *Proceedings of the 1984 International Snow Science Workshop*, ISSW 1994 Organizing Committe, pp. 117–131.

Fischer, J.-T. (2013). A novel approach to evaluate and compare computational snow avalanche simulation. *Natural Hazards and Earth System Sciences*, *13*(6), 1655–1667. https://doi.org/10.5194/nhess-13-1655-2013

Fischer, J.-T., Kofler, A., Fellin, W., Granig, M., & Kleemayr, K. (2015). Multivariate parameter optimization for computational snow avalanche simulation. *Journal of Glaciology*, *61*(229), 875–888. https://doi.org/10.3189/2015JoG14J168

Fischer, J.-T., Kowalski, J., & Pudasaini, S. P. (2012). Topographic curvature effects in applied avalanche modeling. *Cold Regions Science and Technology*, *74–75*, 21–30. https://doi.org/10.1016/j.coldregions.2012.01.005

GDAL Development Team (2016). GDAL-Geospatial Data Abstraction Library, Version GDAL 2.1.0, Open Source Geospatial Foundation.

Gandin, L. S., & Murphy, A. H. (1992). Equitable skill scores for categorical forecasts. *Monthly Weather Review*, *120*(2), 361–370. https://doi.org/10.1175/1520-0493(1992)120<0361:ESSFCF>2.0.CO;2

Harpold, A. A., Kaplan, M. L., Klos, P. Z., Link, T., McNamara, J. P., Rajagopal, S., et al. (2017). Rain or snow: Hydrologic processes, observations, prediction, and research needs. *Hydrology and Earth System Sciences*, *21*(1), 1–22. https://doi.org/10.5194/hess-21-1-2017

Heilig, A., Mitterer, C., Schmid, L., Wever, N., Schweizer, J., Marshall, H.-P., & Eisen, O. (2015). Seasonal and diurnal cycles of liquid water in snow—Measurements and modeling. *Journal of Geophysical Research: Earth Surface*, *120*, 2139–2154. https://doi.org/10.1002/2015JF003593

Hintze, J. L., & Nelson, R. D. (1998). Violin plots: A box plot-density trace synergism. *Journal of the American Statistical Association*, *52*(2), 181–184. https://doi.org/10.1080/00031305.1998.10480559

Hirashima, H., Avanzi, F., & Yamaguchi, S. (2017). Liquid water infiltration into a layered snowpack: Evaluation of a 3-D water transport model with laboratory experiments. *Hydrology and Earth System Sciences*, *21*(11), 5503–5515. https://doi.org/10.5194/hess-21-5503-2017

Kattelmann, R. (1984). Wet slab instability. In *Proceedings of the 1984 International Snow Science Workshop*, ISSW 1984 Workshop Committee, pp. 102–108.

Lehning, M., Völksch, I., Gustafsson, D., Nguyen, T. A., Stähli, M., & Zappa, M. (2006). ALPINE3D: A detailed model of mountain surface processes and its application to snow hydrology. *Hydrological Processes*, *20*(10), 2111–2128. https://doi.org/10.1002/hyp.6204

Leroux, N. R., & Pomeroy, J. W. (2017). Modelling capillary hysteresis effects on preferential flow through melting and cold layered snowpacks. *Advances in Water Resources*, *107*, 250–264. https://doi.org/10.1016/j.advwatres.2017.06.024

Maggioni, M., & Gruber, U. (2003). The influence of topographic parameters on avalanche release dimension and frequency. *Cold Regions Science and Technology*, *37*(3), 407–419. https://doi.org/10.1016/S0165-232X(03)00080-6

McClung, D. M., & Clarke, G. K. C. (1987). The effects of free water on snow gliding. *Journal of Geophysical Research*, *92*(B7), 6301–6309. https://doi.org/10.1029/JB092iB07p06301

McClung, D., & Schaerer, P. A. (2006). *The avalanche handbook* (3rd ed.). Seattle WA, U.S.A: The Mountaineers Books.

Mergili, M., Fischer, J.-T., Krenn, J., & Pudasaini, S. P. (2017). r.avaflow v1, an advanced open-source computational framework for the propagation and interaction of two-phase mass flows. *Geoscientific Model Development*, *10*(2), 553–569. https://doi.org/10.5194/gmd-10-553-2017

Mitterer, C., Heilig, A., Schweizer, J., & Eisen, O. (2011). Upward-looking ground-penetrating radar for measuring wet-snow properties. *Cold Regions Science and Technology*, *69*(2–3), 129–138. https://doi.org/10.1016/j.coldregions.2011.06.003

Mitterer, C., Hirashima, H., & Schweizer, J. (2011). Wet-snow instabilities: Comparison of measured and modelled liquid water content and snow stratigraphy. *Annals Glaciology*, *52*(58), 201–208. https://doi.org/10.3189/172756411797252077

Mitterer, C., & Schweizer, J. (2013). Analysis of the snow-atmosphere energy balance during wet-snow instabilities and implications for avalanche prediction. *Cryosphere*, *7*(1), 205–216. https://doi.org/10.5194/tc-7-205-2013

Mitterer, C., & Schweizer, J. (2014). Comparing models of different levels of complexity for the prediction of wet snow avalanches. In *Proceedings of the International Snow Science Workshop, Banff*, pp. 9–14.

Naaim, M., Durand, Y., Eckert, N., & Chambon, G. (2013). Dense avalanche friction coefficients: Influence of physical properties of snow. *Journal of Glaciology*, *59*(216), 771–782. https://doi.org/10.3189/2013JoG12J205

R Core Team (2015). *R: A language and environment for statistical computing*. Vienna, Austria: R Foundation for Statistical Computing.

Reardon, B., & Lundy, C. (2004). Forecasting for natural avalanches during spring opening of the Going-to-the-Sun road, Glacier National Park, USA, pp. 565–581.

Reiweger, I., Zöchling, M., Forster, M., Wiesinger, T., & Mitterer, C. (2016). Wet-snow fracture propagation. In *Proceedings ISSW 2016, International Snow Science Workshop*, Breckenridge CO, USA. 3–7 October 2016.

Schlögl, S., Marty, C., Bavay, M., & Lehning, M. (2016). Sensitivity of Alpine3D modeled snow cover to modifications in DEM resolution, station coverage and meteorological input quantities. *Environmental Modelling & Software*, *83*, 387–396. https://doi.org/10.1016/j.envsoft.2016.02.017

Schmid, L., Heilig, A., Mitterer, C., Schweizer, J., Maurer, H., Okorn, R., & Eisen, O. (2014). Continuous snowpack monitoring using upward-looking ground-penetrating radar technology. *Journal of Glaciology*, *60*(221), 509–525. https://doi.org/10.3189/2014JoG13J084

Sovilla, B., & Bartelt, P. (2002). Observations and modelling of snow avalanche entrainment. *Natural Hazards and Earth System Sciences*, *2*(3/4), 169–179. https://doi.org/10.5194/nhess-2-169-2002

Sovilla, B., Schaer, M., Kern, M., & Bartelt, P. (2008). Impact pressures and flow regimes in dense snow avalanches observed at the Vallée de la Sionne test site. *Journal of Geophysical Research*, *113*, f01010. https://doi.org/10.1029/2006JF000688

Steinkogler, W., Sovilla, B., & Lehning, M. (2014). Influence of snow cover properties on avalanche dynamics. *Cold Regions Science and Technology*, *97*, 121–131. https://doi.org/10.1016/j.coldregions.2013.10.002

Swiss Avalanche Warning Service (2018). Selected wet snow avalanche activity data Davos, Switzerland (2011–2014), 1, https://doi.org/10.16904/envidat.39, dataset.

Swisstopo (2018a). The digital height model of Switzerland (DHM25), 25 m resolution, (5704 000 000).

Swisstopo (2018b). swissAlti3D, digital height model of Switzerland, 2 m resolution.

Takeuchi, Y., & Hirashima, H. (2013). Snowpack estimations in the starting zone of large-scale snow avalanches in the Makunosawa valley, Myoko, Japan. *Annals Glaciology*, *54*(62), 19–24. https://doi.org/10.3189/2013AoG62A155

Techel, F., & Pielmeier, C. (2009). Wet snow diurnal evolution and stability assessment. In *Proceedings ISSW 2009. International Snow Science Workshop 2009* (pp. 256–261). Davos, Switzerland.

Techel, F., & Pielmeier, C. (2010). Snowpack properties of unstable wet snow slopes: Observations from the Swiss Alps. In *Proceedings ISSW 2010. International Snow Science Workshop 2010* (pp. 187–193). Squaw Valley, CA, USA.

Techel, F., & Pielmeier, C. (2011). Point observations of liquid water content in wet snow—Investigating methodical, spatial and temporal aspects. *Cryosphere*, *5*(2), 405–418. https://doi.org/10.5194/tc-5-405-2011

Techel, F., & Pielmeier, C. (2013). Schnee und Lawinen in den Schweizer Alpen. Hydrologisches Jahr 2010/11, 95 pp., WSL-Institut für Schnee- und Lawinenforschung SLF Davos, in German.

Techel, F., Pielmeier, C., Darms, G., Teich, M., & Margreth, S. (2013). Schnee und Lawinen in den Schweizer Alpen. Hydrologisches Jahr 2011/121, 118 pp., WSL-Institut für Schnee- und Lawinenforschung SLF Davos (WSL Ber. 5), in German.

Techel, F., Pielmeier, C., & Schneebeli, M. (2011). Microstructural resistance of snow following first wetting. *Cold Regions Science and Technology*, *65*(3), 382–391. https://doi.org/10.1016/j.coldregions.2010.12.006

Techel, F., Stucki, T., Margreth, S., Marty, C., & Winkler, K. (2015). Schnee und Lawinen in den Schweizer Alpen. Hydrologisches Jahr 2013/14, 87 pp., WSL-Institut für Schnee- und Lawinenforschung SLF Davos (WSL Ber. 31), in German.

Techel, F., Zweifel, B., & Winkler, K. (2015). Analysis of avalanche risk factors in backcountry terrain based on usage frequency and accident data in Switzerland. *Natural Hazards and Earth System Sciences*, *15*(9), 1985–1997. https://doi.org/10.5194/nhess-15-1985-2015

Teich, M., Fischer, J.-T., Feistl, T., Bebi, P., Christen, M., & Grêt-Regamey, A. (2014). Computational snow avalanche simulation in forested terrain. *Natural Hazards and Earth System Sciences*, *14*(8), 2233–2248. https://doi.org/10.5194/nhess-14-2233-2014

Veitinger, J., Purves, R. S., & Sovilla, B. (2016). Potential slab avalanche release area identification from estimated winter terrain: A multi-scale, fuzzy logic approach. *Natural Hazards and Earth System Sciences*, *16*(10), 2211–2225. https://doi.org/10.5194/nhess-16-2211-2016

Veitinger, J., Sovilla, B., & Purves, R. S. (2014). Influence of snow depth distribution on surface roughness in alpine terrain: a multi-scale approach. *Cryosphere*, *8*(2), 547–569. https://doi.org/10.5194/tc-8-547-2014

Vera Valero, C., Wever, N., Bühler, Y., Stoffel, L., Margreth, S., & Bartelt, P. (2016). Modelling wet snow avalanche runout to assess road safety at a high-altitude mine in the central Andes. *Natural Hazards and Earth System Sciences*, *16*(11), 2303–2323. https://doi.org/10.5194/nhess-16-2303-2016

Vera Valero, C., Wever, N., Christen, M., & Bartelt, P. (2018). Modeling the influence of snow cover temperature and water content on wet-snow avalanche runout. *Natural Hazards and Earth System Sciences*, *18*(3), 869–887. https://doi.org/10.5194/nhess-18-869-2018

Vera Valero, C., Wikstroem Jones, K., Bühler, Y., & Bartelt, P. (2015). Release temperature, snow-cover entrainment and the thermal flow regime of snow avalanches. *Journal of Glaciology*, *61*(225), 173–184.

Vögeli, C., Lehning, M., Wever, N., & Bavay, M. (2016). Scaling precipitation input to spatially distributed hydrological models by measured snow distribution. *Frontiers of Earth Science*, *4*, 108. https://doi.org/10.3389/feart.2016.00108

WSL Institute for Snow and Avalanche Research SLF (2015). Meteorological and snowpack measurements from Weissfluhjoch, Davos, Switzerland, 1. https://doi.org/10.16904/1, dataset.

Wever, N., Comola, F., Bavay, M., & Lehning, M. (2017). Simulating the influence of snow surface processes on soil moisture dynamics and streamflow generation in an alpine catchment. *Hydrology and Earth System Sciences*, *21*(8), 4053–4071. https://doi.org/10.5194/hess-21-4053-2017

Wever, N., Fierz, C., Mitterer, C., Hirashima, H., & Lehning, M. (2014). Solving Richards equation for snow improves snowpack meltwater runoff estimations in detailed multi-layer snowpack model. *Cryosphere*, *8*(1), 257–274. https://doi.org/10.5194/tc-8-257-2014

Wever, N., Schmid, L., Heilig, A., Eisen, O., Fierz, C., & Lehning, M. (2015). Verification of the multi-layer SNOWPACK model with different water transport schemes. *Cryosphere*, *9*(6), 2271–2293. https://doi.org/10.5194/tc-9-2271-2015

Wever, N., Vera Valero, C., & Fierz, C. (2016). Assessing wet snow avalanche activity using detailed physics based snowpack simulations. *Geophysical Research Letters*, *43*, 5732–5740. https://doi.org/10.1002/2016GL068428

Wever, N., Würzer, S., Fierz, C., & Lehning, M. (2016). Simulating ice layer formation under the presence of preferential flow in layered snowpacks. *Cryosphere*, *10*(6), 2731–2744. https://doi.org/10.5194/tc-10-2731-2016

Würzer, S., Jonas, T., Wever, N., & Lehning, M. (2016). Influence of initial snowpack properties on runoff formation during rain-on-snow events. *Journal of Hydrometeorology*, *17*(6), 1801–1815. https://doi.org/10.1175/JHM-D-15-0181.1

Würzer, S., Wever, N., Juras, R., Lehning, M., & Jonas, T. (2017). Modelling liquid water transport in snow under rain-on-snow conditions—Considering preferential flow. *Hydrology and Earth System Sciences*, *21*(3), 1741–1756. https://doi.org/10.5194/hess-21-1741-2017

Yamaguchi, S., Watanabe, K., Katsushima, T., Sato, A., & Kumakura, T. (2012). Dependence of the water retention curve of snow on snow characteristics. *Ann. Glaciol.*, *53*(61), 6–12. https://doi.org/10.3189/2012AoG61A001

Yamanoi, K., & Endo, Y. (2002). Dependence of shear strength of snow cover on density and water content. *Seppyo*, *64*(4), 443–451. in Japanese with English Abstract.

Zischg, A., Fuchs, S., Keiler, M., & Meißl, G. (2005). Modelling the system behaviour of wet snow avalanches using an expert system approach for risk management on high alpine traffic roads. *Natural Hazards and Earth System Sciences*, *5*(6), 821–832. https://doi.org/10.5194/nhess-5-821-2005